Magma mixing origin for high Ba–Sr granitic pluton in the Bayankhongor area, central Mongolia: Response to slab roll-back

Yunying Zhang [a,b], Min Sun [c], Chao Yuan [a,*], Yigang Xu [a], Xiaoping Long [a], Dondov Tomurhuu [d], Christina Yan Wang [a], Bin He [a]

[a] State Key Laboratory of Isotope Geochemistry, Guangzhou Institute of Geochemistry, Chinese Academy of Sciences, Guangzhou 510640, China
[b] University of Chinese Academy of Sciences, Beijing 10069, China
[c] Department of Earth Sciences, The University of Hong Kong, Pokfulam Road, Hong Kong, China
[d] Institute of Geology and Mineral Resources, Mongolian Academy of Sciences, Ulaanbaatar 210351, Mongolia

ARTICLE INFO

ABSTRACT

Petrogenesis of high Ba–Sr granitoids is a matter of debate. This paper presents whole-rock geochemical, Sr–Nd isotopic and zircon U–Pb and Hf isotopic data for a suite of high Ba–Sr biotite monzogranite and associated mafic microgranular enclaves (MMEs) from the Ulaan Uul batholith in the Bayankhongor area, central Mongolia, aiming at elucidating the complex petrogenesis of the high Ba–Sr granitoids. The data manifest that magma mixing between a felsic magma derived from sedimentary rocks and a mafic magma derived from Sub-Continental lithospheric mantle (SCLM) may account for the formation of high Ba–Sr granitoids. The host granite and MMEs yielded U–Pb ages of 546 ± 3 Ma and 547 ± 3 Ma, respectively, suggesting that the mafic and felsic magmas were coeval. Rocks of the host granitoids possess high SiO_2 and low MgO contents and display peraluminous high-K calc-alkaline and shoshonitic characteristics. Their relatively high Ba, Sr but low HREE (Yb < 2 ppm) resemble those of typical high Ba–Sr granitoids. Rocks from the granitoids have crust-like Sr–Nd isotopic compositions [$(^{87}Sr/^{86}Sr)_i$ = 0.7059–0.7065, and $\varepsilon Nd(t)$ = −1.8 to −2.1], and most zircons from the host rocks show negative $\varepsilon Hf(t)$ values (−0.63 to −11.9) with two-stage Hf model ages of 1.54–2.25 Ga. The MMEs have low SiO_2 and high MgO concentrations, enriched Sr–Nd isotopic compositions [$(^{87}Sr^{86}Sr)_i$ = 0.7060–0.7066, and $\varepsilon Nd(t)$ = −1.6 to −2.1], and most zircons from the MMEs have positive $\varepsilon Hf(t)$ values (+0.7 to +2.6), with late Mesoproterozoic single-stage Hf model ages (1.05–1.12 Ga), suggesting an origin of late Mesoproterozoic SCLM. We interpret that the Ulaan Uul batholith has a mixed origin, i.e. partial melting of sedimentary rocks triggered by upwelling of lithospheric mantle-derived magma (represented by MMEs) under an extensional scheme, and subsequent mixing of the mantle- and crust-derived melts resulted in the high Ba–Sr granitoids. We speculate that the late Neoproterozoic to early Cambrian extensional environment in the Bayankhongor area was caused by the roll-back of subducting Bayankhongor oceanic lithosphere.

© 2014 Elsevier Ltd. All rights reserved.

1. Introduction

High Ba–Sr granitoids were originally recognized by Tarney and Jones (1994) in the Scottish Caledonides and received wide attention (Eklund et al., 1998; Fowler et al., 2001, 2008; Qian et al., 2003; Choi et al., 2009; Yuan et al., 2010; Bruand et al., 2014). Rocks of this kind are characterized by high Ba (>500 ppm) and Sr (>300 ppm), which are distinct from typical I-, S- and A-type granitoids (Tarney and Jones, 1994). Petrogenesis of high Ba–Sr granitoids has been extensively studied, but no consensus has been

reached, and a variety of petrogenetic models have been proposed, including: (1) partial melting of subducted ocean plateaus (Tarney and Jones, 1994); (2) partial melting of mafic lower crust (Ye et al., 2008; Choi et al., 2009); (3) partial melting of enriched lithospheric mantle metasomatized by asthenosphere-derived carbonatitic melts or subduction-related fluids and/or melts (Eklund et al., 1998; Fowler et al., 2001, 2008; Peng et al., 2013). High Ba–Sr granitoids commonly contain mafic microgranular enclaves (MMEs) which have complex origins such as restites (Chappell and White, 1992; White et al., 1999), cumulates formed by early-stage crystallization (Didier and Barbarin, 1991; Dahlquist, 2002; Donaire et al., 2005) and inclusions of mantle-derived magma (Vernon, 1984; Griffin et al., 2002; Barbarin, 2005; Yang et al.,

2007). The MMEs can provide important information on the source nature and geodynamic setting as well as crust–mantle interaction processes of the granitoids.

The Central Asian Orogenic Belt (CAOB) (Sengör et al., 1993; Sengör and Natal'in, 1996; Jahn et al., 2000; Khain et al., 2003; Xiao et al., 2004) extends from the Urals in the west, through Kazakhstan, Kyrghyzstan, NW China, and southern Mongolia to the Pacific coast in the east. It experienced multiple subduction–accretion and collisional processes and consists mainly of accreted fragments including island arcs, accretionary complexes, seamounts, ophiolites and microcontinents (Kröner et al., 2007; Windley et al., 2007; Xiao et al., 2008). Distinct from the past cognition that the CAOB was formed by southward growth of juvenile terranes through subduction–accretion (e.g. Sengör and Natal'in, 1996; Windley et al., 2007; Xiao et al., 2009), a mechanism of northeastward growth of accretionary complexes as a result of southward subduction has been proposed to account for the formation of the Bayankhongor region in the central Mongolia (Figs. 1 and 2) (Buchan et al., 2001). During the evolution of the Bayankhongor region, extensive felsic and mafic magmas were produced, including high Ba–Sr granitoids and mafic enclaves (Buchan et al., 2002; Jahn et al., 2004; Demoux et al., 2009), and can provide important constraints on the evolutionary history of the Bayankhongor region. Recent research in the Bayankhongor region mostly focused on the accretionary complexes, however, little is known regarding the geodynamic and genetic relationships between high Ba–Sr granitoids and associated MMEs.

In this contribution, we report new U–Pb zircon ages, whole rock major and trace element and Sr–Nd–Hf isotopic compositions for a Precambrian high Ba–Sr granitoid pluton (the Ulaan Uul batholith) and associated MMEs, aiming to (1) investigate the petrogenesis and genetic relationship between the host granite and associated MMEs; (2) constrain the accretionary process of the Bayankhongor region in more detail.

2. Geological background and sample descriptions

2.1. Geological background

As a part of the CAOB, Mongolia experienced multiple subduction and collisional events as a consequence of the consumption of the Paleo–Asian Ocean (Fig. 1) (Badarch et al., 2002). Tectonically, Mongolia can be divided into the southern and northern domains separated by the Main Mongolian Lineament which marked a late Orodovician plate boundary (Lehmann et al., 2010). The southern domain is dominated by middle to late Paleozoic accretionary complexes, whereas the northern domain mainly comprises Precambrian to early Paleozoic metamorphic rocks, Neoproterozoic ophiolitic belts and early Paleozoic arc-related volcanic rocks (Buchan et al., 2001, 2002; Jiang et al., 2012). The Bayankhongor region in the northern domain is sandwiched between the Baydrag microcontinent in the south and the Hangay microcontinent in the north (Fig. 2) (Jahn et al., 2004; Jian et al., 2010). Previous workers divided the Bayankhongor region into several tectonic subunits, i.e., from south to north the Baydrag microcontinent, the Burd Gol mélange, the South Volcanic Belt, the Bayankhongor suture zone and the Dzag zone of the Hangay microcontinent (Fig. 2) (Buchan et al., 2001, 2002).

The basement of the Baydrag microcontinent is mainly composed of Neoarchean to Paleoproterozoic tonalitic to granitic gneisses which have underwent amphibolite- and granulite-facies metamorphism (Mitrofanov et al., 1985; Kotov et al., 1995; Teraoka et al., 1996; Kozakov et al., 2001; Demoux et al., 2009). To the northeast of the Baydrag block, the Burd Gol mélange represents a subduction–accretion complex and comprises phyllites, slates, chlorite–biotite schists which probably deposited in the earliest Neoproterozoic (Demoux et al., 2009). Moreover, this mélange underwent Barrovian-type metamorphism with metamorphic grade increasing northwards, and the time of metamorphism can
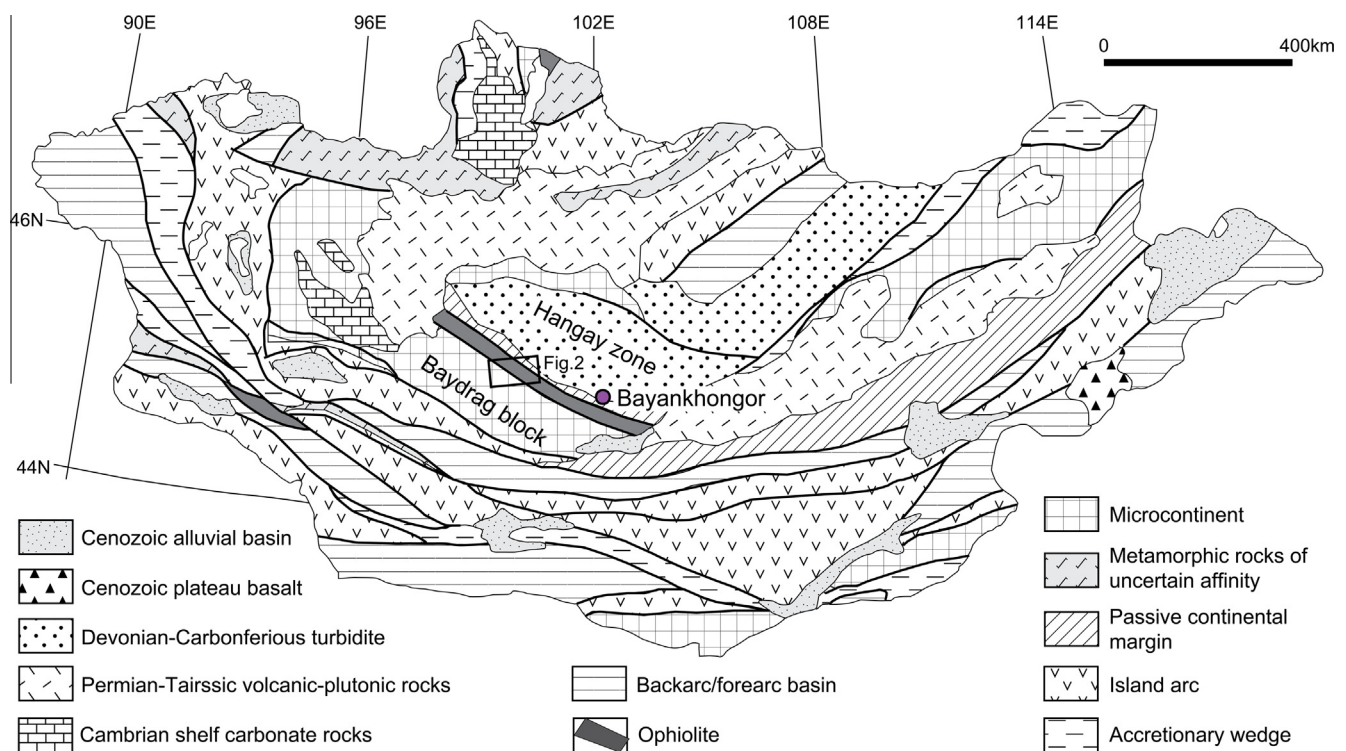

Fig. 1. Simplified terrane map of Mongolia (modified after Badarch et al., 2002).
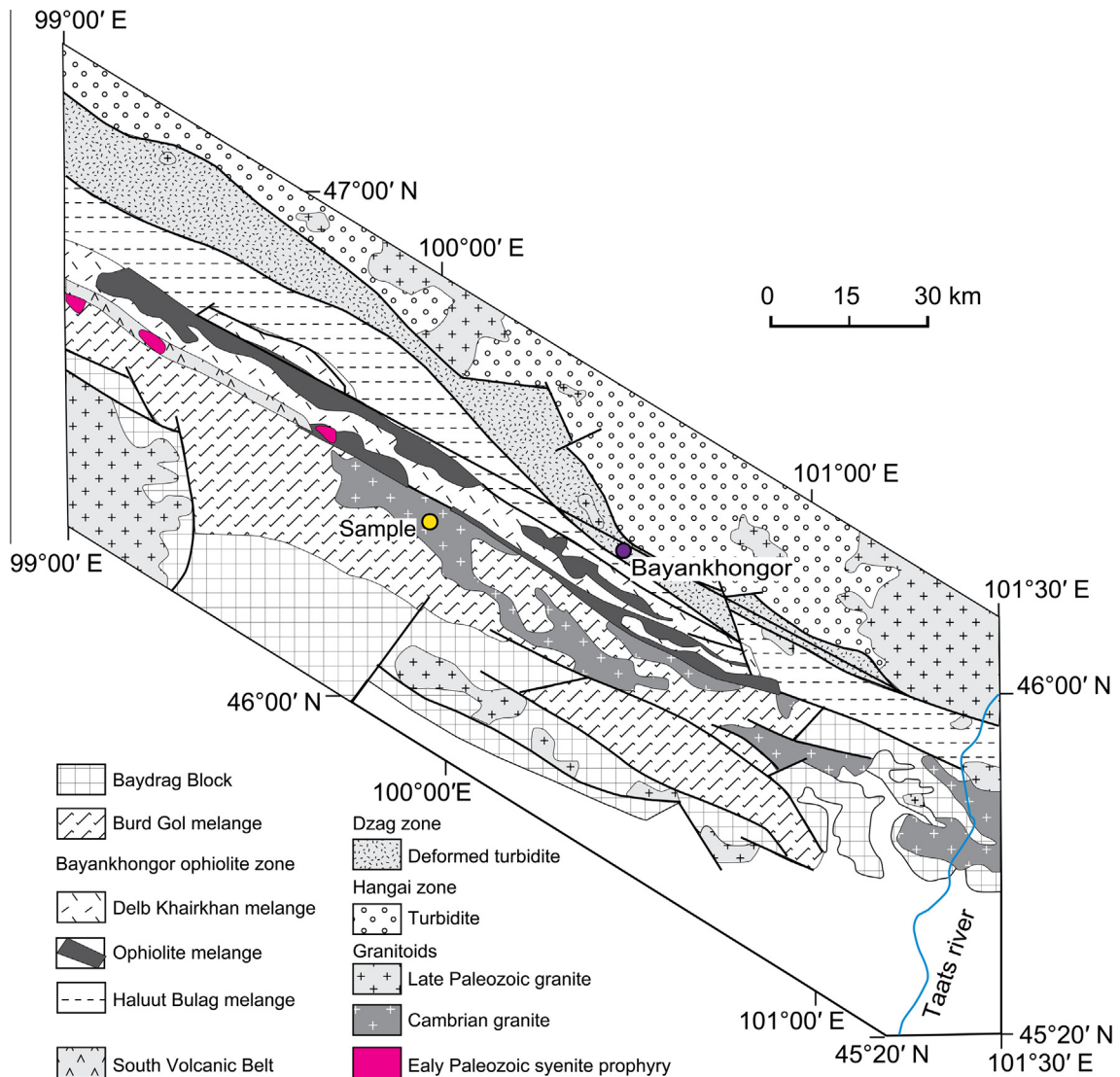
Fig. 2. Geological map of the Bayankhongor region (modified after Jian et al., 2010). The position of analyzed samples is also marked.

be roughly bracketed between ca. 562 and ca. 533 Ma (Höck et al., 2000; Kozakov et al., 2006). The South Volcanic Belt consists mainly of late Neoproterozoic to early Paleozoic arc-related volcanic rocks (Kröner et al., 2011). The Bayankhongor suture zone can be divided into three subunits, which are, from south to north, the Delb Khairkhan mélange, the Bayankhongor ophiolitic mélange and the Haluut Bulag mélange (Buchan et al., 2002) (Fig. 2). The Delb Khairkhan mélange is dominated by pelitic schists and has been considered to be middle Neoproterozoic to early Paleozoic in age based on the presence of Neoproterozoic stromatolites and Cambrian fossils (Dergunov et al., 1997). The Bayankhongor ophiolitic mélange comprises ultramafic cumulates, gabbros, pillow lavas and sheeted dykes which have been tectonically dismembered into slices enclosed in a matrix of serpentinite (Buchan et al., 2002). Zircons from ophiolitic anorthosite, gabbro and plagiogranite yielded late Neoproterozoic $^{207}Pb/^{206}Pb$ ages ranging from 655 ± 4 to 636 ± 6 Ma (Jian et al., 2010). The Haluut Bulag mélange contains lenticular mudstone, limestone, sandstone and locally vesicular basalt enclosed in a matrix of pelitic schist (Buchan et al., 2001). Although no precise age is reported, the presence of radiolarian fossils in Cambrian sediments indicates that the depositional age of the Haluut Bulag mélange is no older than Cambrian (542 Ma) (Osozawa et al., 2008). The Dzag zone of the

Hangay microcontinent comprises greenschist–facies psammitic and pelitic schists which probably deposited on the passive margin of the Hangay microcontinent to the north (Kurimoto et al., 1998; Buchan et al., 2001).

2.2. Granitoid intrusions

Voluminous late Neoproterozoic to early Cambrian granitoids intruded the Bayankhongor region (Fig. 2). For example, Buchan et al. (2002) reported zircon evaporation $^{207}Pb/^{206}Pb$ ages of 539 ± 5 Ma for a granitic pluton that intruded the Burd Gol mélange. A syenite porphyry intruding the Burd Gol mélange yielded a SHRIMP zircon age of 523 ± 2 Ma (Jian et al., 2010). In addition, several zircon U–Pb ages (520–565 Ma) have been reported for granitic intrusions along the Taats River (Fig. 2), which has been considered as the eastern extension of the Baydrag block (Kozakov et al., 2006, 2008; Demoux et al., 2009).

In this study, we focus on the Ulaan Uul batholith, whose majority intrudes the northern margin of the Burd Gol mélange (Fig. 2). Outcrops of this batholith can also be found in the Delb Khairkhan mélange and the Bayankhongor ophiolitic mélange. This batholith has been considered to be early Cambrian in age based on two zircon evaporation $^{207}Pb/^{206}Pb$ ages of 539 ± 1 and 545 ± 2 Ma (Buchan

et al., 2002). The body is composed mainly of biotite monzogranite with rounded mafic microgranular enclaves, and has medium-grained granular textures (Fig. 3a). The main minerals are plagioclase (35–45 vol.%), alkali–feldspar (25–35 vol.%), quartz (20–25 vol.%), and biotite (~5 vol.%), with minor titanite, apatite and zircon. Enclaves within the batholith are fine-grained and ellipsoidal with size ranging from 10 to 30 cm, and generally show porphyritic or equigranular textures (Fig. 3a and b). The contact between the enclaves and host rocks are mostly sharp, though gradational contact can be observed locally. The enclaves are mainly dioritic in lithology and consist of plagioclase (35–40 vol.%), hornblende (30–35 vol.%), K-feldspar (10–15 vol.%), biotite (5–10 vol.%), with minor apatite (Fig. 3a and b). Except for a few that show gradational contact with the host, most enclaves do not contain K-feldspar megacrysts.

3. Analytical methods

All geochemical analysis of zircon U–Pb dating, whole rock geochemistry, Sr–Nd–Hf isotopic compositions, were carried out at the State Key Laboratory of Isotope Geochemistry, Guangzhou Institute of Geochemistry, Chinese Academy of Sciences (SKLIG GIG CAS).

3.1. Zircon U–Pb dating

Zircons were separated from two samples (one from the Ulaan Uul batholith and one from mafic enclave) using conventional heavy liquid and magnetic separation techniques and then were hand-picked under a binocular microscope. Representative zircon grains were mounted in epoxy resin discs, then polished to about half of their thickness and coated with carbon. Cathodoluminescence (CL) images of zircons were obtained at SKLIG GIG CAS using a JEOL JXA-8100 Electron Probe Microanalyzer with a Mono CL3 CL System for inspecting internal morphology of zircons. Zircon U–Pb dating was carried out by using Laser ablarion ICP–MS. NIST SRM 610 and Temora zircon standards were used as external standards. Detailed operating conditions for the laser ablation system and the ICP–MS instrument and data reduction can be found in Li et al. (2011).

3.2. Whole-rock geochemistry and Sr–Nd isotope analyses

Major element compositions were measured on fused glass disks using X-ray fluorescence spectrometry (Rigaku ZSX100e)

following analytical procedures described by Li et al. (2006) and analytical precision for major elements was between 1% and 5%. Trace elements analyses were performed using a Perkin–Elmer Sciex ELAN 6000 inductively coupled plasma mass spectrometry (ICP–MS). Sample powders were digested using an HF + HNO$_3$ mixture in high pressure Teflon bombs for two days in order to assure complete dissolution of the refractory minerals. USGS rock standards and Chinese national rock standards (GSR-1, GSR-2, GSR-3, GSD-9) were used to calibrate elemental concentrations of the measured samples. The analytical procedures are referred to Li et al. (2002), and analytical precision was generally better than 5%. Sr and Nd isotopic analyses were performed on a Micromass Isoprobe multi-collector mass spectrometer (MC–ICP–MS) at SKLIG GIG CAS, following the procedures described by Li et al. (2004). Measured $^{143}Nd/^{144}Nd$ and $^{87}Sr/^{86}Sr$ ratios were normalized to $^{146}Nd/^{144}Nd = 0.7219$ and $^{86}Sr/^{88}Sr = 0.1194$, respectively. The $^{87}Sr/^{86}Sr$ ratio of the NBS987 standard and $^{143}Nd/^{144}Nd$ ratio of the Shin Etsu JNdi-1 standard measured during this study were 0.710256 ± 22 ($2\sigma m$) and 0.512110 ± 8 ($2\sigma m$), respectively.

3.3. Zircon Lu–Hf isotope analyses

In situ zircon Hf isotopic analysis was carried out using the Neptune Plus MC–ICP–MS, attached to the Resonetics RESOlution M-50-LR Excimer Laser Ablation System at SKLIG GIG CAS. During the analyses, a laser repetition rate of 8 Hz at 80 mJ was used for ablating zircons, and spot size was 45 μm. The ablated material was transported in a helium carrier gas with addition of a small flow of nitrogen. Data acquisition for each analysis consists of 30 s gas background collection and 30 s signal collection for laser ablation. A signal collection model for one block includes 200 cycles, in which one cycle has 0.131 s integration time. The measured isotopic ratios of $^{176}Hf/^{177}Hf$ were normalized to $^{176}Hf/^{177}Hf = 0.7325$, using an exponential correction for mass bias. Correction for isobaric interference of ^{176}Lu on ^{176}Hf and ^{176}Yb on ^{176}Hf was performed using the recommended $^{176}Lu/^{175}Lu$ ratio of 0.02655 (Machado and Simonetti, 2001) and $^{176}Yb/^{171}Yb$ ratio of 0.90184. Penglai zircons were used as reference standards and were analyzed twice before and after every 5 analyses. Repeated measurements of this zircon standard during our study yielded $^{176}Hf/^{177}Hf = 0.282891 \pm 0.000012$ (2σ, $n = 22$), which is identical to the previously reported literature values (Li et al., 2010). The ^{176}Lu decay constant of 1.867×10^{-11} year^{-1} (Soderlund et al.,
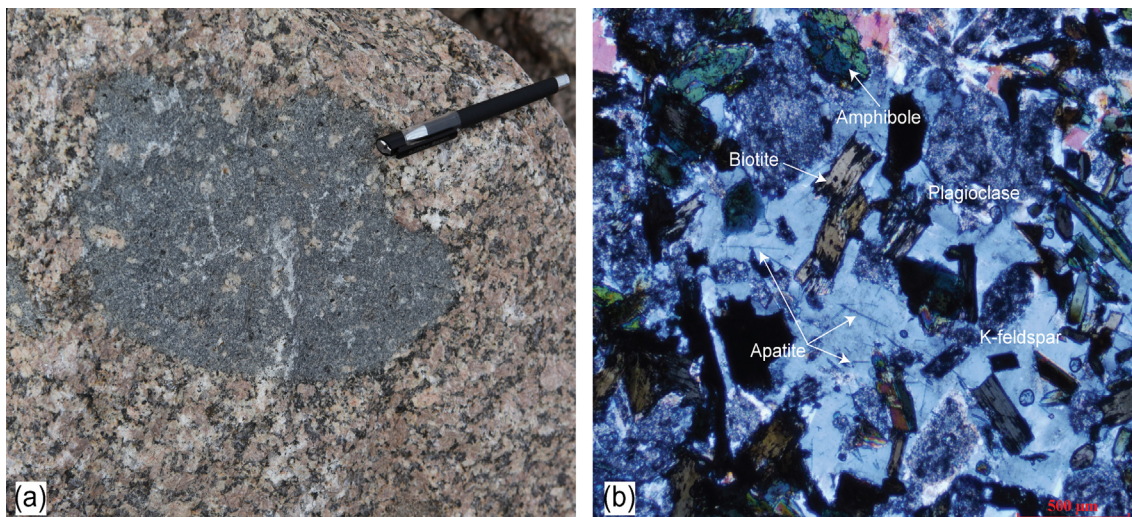

Fig. 3. (a) Field photograph showing the relationship between the host granite and MMEs; (b) photomicrograph showing the main textures and mineral assemblages of the MME.

2004) was used to calculate initial ^{176}Hf/^{177}Hf ratios. The chondritic values of ^{176}Hf/^{177}Hf (0.282772) and ^{176}Lu/^{177}Hf (0.0332) reported by (Blichert-Toft and Albarede, 1997) were adopted for the calculation of εHf values. Single-stage Hf model ages (T_{DM1}) were calculated relative to the depleted mantle present-day value of ^{176}Hf/^{177}Hf = 0.283250 and ^{176}Lu/^{177}Hf = 0.0384 (Griffin et al., 2000). Two-stages "crustal" model ages (T_{DM2}) were calculated using the mean ^{176}Lu/^{177}Hf ratio of 0.015 for the average continental crust (Griffin et al., 2002).

4. Analytical results

4.1. Geochronology

LA–ICP–MS zircon U–Pb isotope analytical results of the host granite and associated MME can be found in Appendix 1. Zircons from the host granite (MG11-89-11) are prismatic and transparent with well-developed oscillatory zoning, indicating a magmatic origin. Size of the zircons ranges from 100 to 200 μm in length, with length/width ratios of 2:1 to 4:1 (Fig. 4a). The analyzed zircons have intermediate Th (27–523 ppm) and U (41–421 ppm) contents with Th/U ratios of 0.29 to 1.33, consistent with an igneous origin. Twenty-seven analyses were obtained and form a coherent group with a weighted mean ^{206}Pb/^{238}U age of 546 ± 3 Ma (Fig. 5b). The age is consistent with previous zircon evaporation ^{207}Pb/^{206}Pb ages (539 ± 1 Ma and 545 ± 2 Ma) (Buchan et al., 2002), and is considered to be the crystallization age of the Ulaan Uul batholith.

Zircons from the MME (MG11-89-1) are stubby to prismatic and grayish dark in color, and have weakly oscillatory zoning. The zircons range in size from 50 to 200 μm in length, with length/width ratios of 1:1 to 3:1 (Fig. 4b). The analyzed zircons have variable Th (29–814 ppm) and U (69–537 ppm) contents with Th/U ratios of

0.28–1.51, indicating a magmatic origin. No inherited cores were found. Seventeen analyses of zircons form a coherent group on the Concordia diagram with a weighted mean ^{206}Pb/^{238}U age of 547 ± 3 Ma (Fig. 5a), which represents the crystallization age of the mafic enclaves. This age is consistent with the U–Pb ages for the host biotite monzogranite, suggesting that the MMEs and their host were coeval mafic and felsic magmatism.

4.2. Major and trace elements

Major and trace element data for the host granite and MMEs are listed in Table 1. Samples from the host biotite monzogranite display high SiO$_2$ (66.0–75.4 wt.%), low MgO (0.55–1.47 wt.%) and TiO$_2$ (0.23–0.64 wt.%) contents (Fig. 7). The host samples are characterized by high total alkali (K$_2$O + Na$_2$O = 7.1–10.0 wt.%) (Fig. 6a) and K$_2$O/Na$_2$O (0.7–1.7), showing high-K calc-alkaline to shoshonitic characteristics (Fig. 6b). Rocks from the host granite are strongly peraluminous with ASI values ranging from 1.10 to 1.17 (Fig. 6c). Rocks of the biotite monzogranite contain high Ba (1189–2544 ppm), Sr (440–742 ppm) and low Yb (<2.1 ppm) and Ta (<2.2 ppm) contents. In addition, they exhibit high K/Rb (354–418), Sr/Y (30–75) and La/Yb (21–91), and low Rb/Ba (<0.07) and Rb/Sr (<0.27) ratios. The rocks are characterized by enrichment of LREE and display slight HREE fractionation (($La/Yb)_N$ = 14.8–64.9; $(Gd/Yb)_N$ = 2.0–2.6) (Fig. 8b), with slightly to moderate negative Eu anomalies (Eu/Eu* = 0.65–0.98). On the primitive mantle-normalized trace element diagram, the biotite monzogranite samples show relative enrichment in LILEs (such as Rb, Ba) and depletion in HFSEs (such as Nb, Ta, Ti) (Fig. 8d).

The MMEs are mafic to intermediate in composition with SiO$_2$ ranging from 52.1 to 67.6 wt.% (Fig. 6a). The MME samples have variable MgO (1.3–3.7 wt.%), Al$_2$O$_3$ (14.7–19.1 wt.%) and TiO$_2$
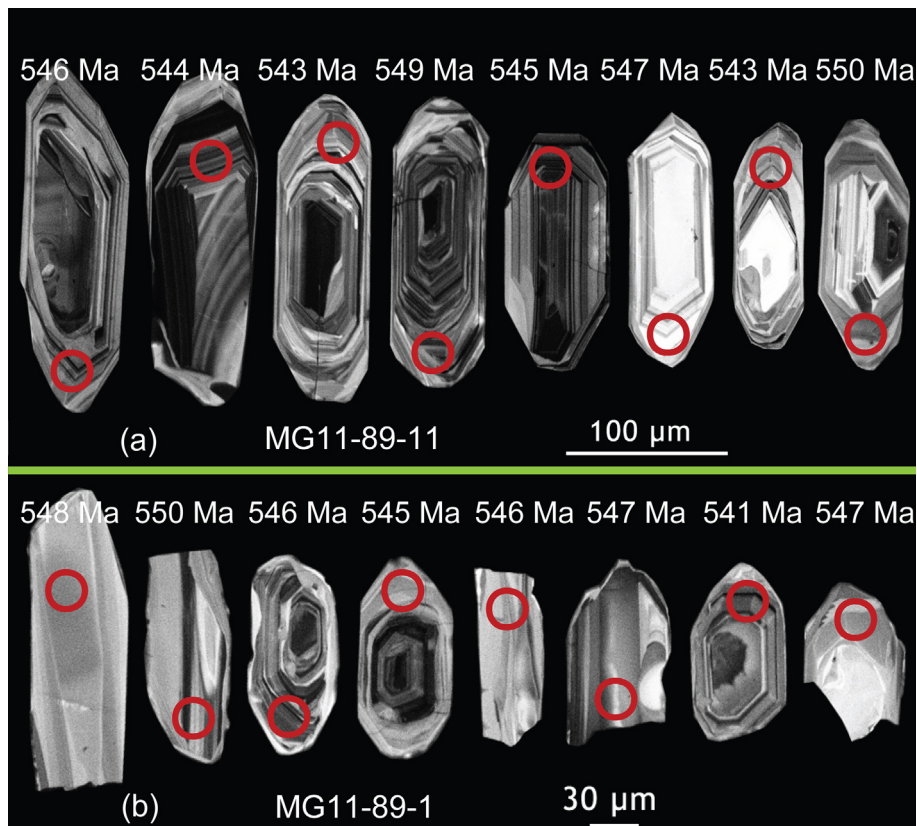

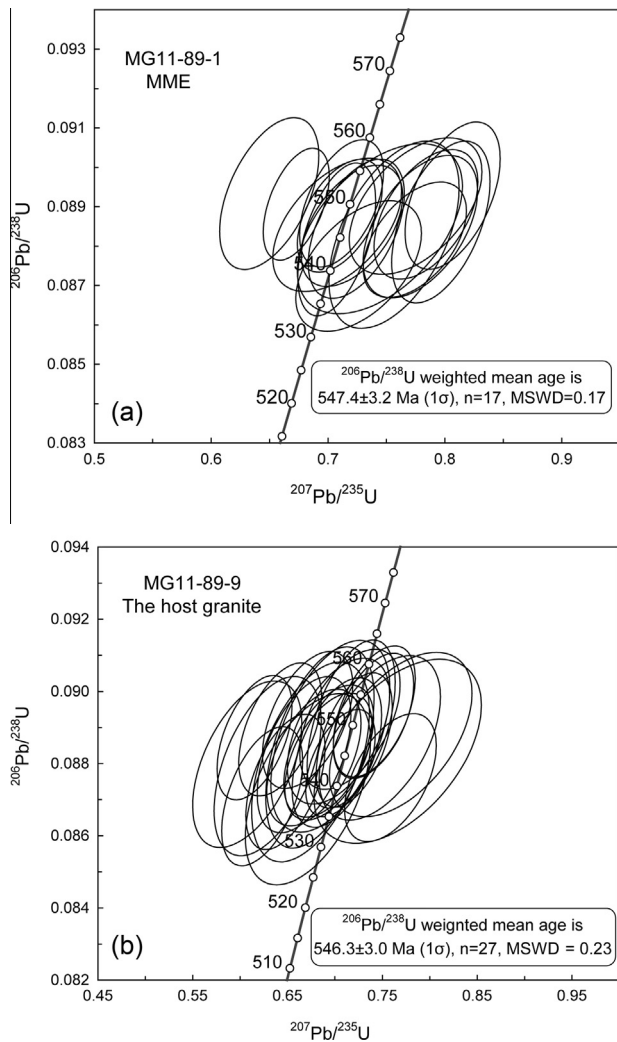Fig. 4. CL images of representative zircons from the host granite (a) and associated MME (b).

Fig. 5. Zircon U–Pb Concordia diagrams and weighted mean ^{206}Pb/^{238}U ages for the MME (a) and host granite (b).

(0.7–1.6 wt.%) contents (Fig. 7), characterized by high total alkali contents (K$_2$O + Na$_2$O = 5.8–8.3 wt.%) (Fig. 6a). The MME rocks are metaluminous to slightly peraluminous (ASI = 0.88–1.05, mostly <1) (Fig. 6c), and relatively Na-enriched as indicated by their high Na$_2$O/K$_2$O ratios (1.1–2.5, mostly >1.8). Rocks of the MMEs have high concentrations of Sr (772–907 ppm), and highly variable Y (9.1–64.5 ppm), Nb (10.5–52.5) contents and Sr/Y (12–87) ratios. The MME samples are characterized by variable LREE enrichment ((La/Yb)$_N$ = 4.8–39.4) and HREE fractionation ((Gd/Yb)$_N$ = 1.4–3.1), with moderate negative Eu anomalies (Eu/Eu* = 0.51–0.75) (Fig. 8a). On the primitive mantle-normalized trace element diagram, the MME samples show relative enrichment in large ion lithophile element (LILE, e.g. Rb, Ba), and variable depletion in high field-strength element (HFSE, e.g. Nb, Ta, Zr) as suggested by their variable Nb/La ratios (0.15–1.27) (Fig. 8c).

4.3. Sr–Nd isotopic compositions

The Sr–Nd isotope compositions of the host granite and MMEs are presented in Table 2 and Fig. 9a. Samples from the host granite have a narrow range of initial ^{87}Sr/^{86}Sr ratios (0.7059–0.7065) and εNd(t) (−1.8 to −2.1) with Nd model ages (T$_{DM}$) of 1.43–1.45 Ga. The MMEs also have uniform initial ^{87}Sr/^{86}Sr ratios (0.7060–

0.7066) and εNd(t) (−1.6 to −2.1), and Nd model ages (T$_{DM}$) of 1.41–1.45 Ga, overlapping the range of the host granite samples.

4.4. Zircon Hf isotopic compositions

In situ zircon Hf isotopic composition for the host granite and MME samples are listed in Appendix 2 and presented in Fig. 10. Except for two zircons from the host granite display positive εHf(t) values (+0.12 and +1.4) with single-stage Hf model ages of 1.08 and 1.13 Ga, the rest twenty-four zircons from the host rock all show variably negative εHf(t) values (−0.63 to −11.9) with two-stage Hf model ages of 1.54–2.25 Ga. Zircons from the MME have higher ^{176}Hf/^{177}Hf ratios and εHf(t) values than those of the host granite samples. Ten of the seventeen analyzed zircons from MME have positive εHf(t) values (+0.7 to +2.6) with single-stage Hf model ages of 1.05–1.12 Ga, and seven MME zircons have negative εHf(t) values (−0.75 to −3.5) with two-stage Hf model ages of 1.51–1.72 Ga.

5. Discussion

5.1. Magma mixing

The igneous texture of the MMEs indicates a magmatic origin (Fig. 3b). In addition, zircon U–Pb dating suggests that the MMEs were coeval with the host granite, thus an origin of xenolith captured from the wall–rock can be precluded. Recently, a cognate origin of MMEs (e.g., early-stage cumulates or differentiation) has been proposed (Dahlquist, 2002; Donaire et al., 2005). Although the similar zircon U–Pb ages of the MMEs and host granite may imply a cogenetic suite, their different zircon Hf isotopic compositions suggest different origins for the MMEs and host granite. In fact, the MMEs have higher total REE contents (mostly >230 ppm) than the host granite samples (mostly <230 ppm), thus precluding an origin of early-stage differentiation product from a cognitive magma. Moreover, some workers proposed that MMEs represent residual materials (restite) successively immixing with the melt (Chappell and White, 1992; White et al., 1999). In this case, MMEs should share similar isotopic compositions to the host granitoids. Although having Sr–Nd isotopic compositions similar to their host (Fig. 9a), the MMEs in the Ulaan Uul batholith display different ^{176}Hf/^{177}Hf ratios and εHf(t) values from those of the host granite (Fig. 10), which, together with their igneous texture (Fig. 3b), argues against a restite origin. Similar whole-rock Sr–Nd isotopes and distinct zircon Hf isotopes between the host granite and associated MMEs, pointing to somewhat Nd–Hf isotope decoupling, have been served as a powerful evidence for crust–mantle magma mixing (Kemp et al., 2005, 2007; Yang et al., 2007; Qin et al., 2009). Generally, chemical equilibrium and isotopic equilibrium can be achieved by elemental diffusion during the magma mixing process (Karsli et al., 2007). The MMEs share similar Sr–Nd isotopic compositions to the host (Fig. 9a), which can be explained by sufficient diffusion exchange with the granitic melt (Qin et al., 2009). However, as a resistant and refractory mineral, zircon commonly crystallizes in the early stage of magmatism, probably prior to the homogenization of mixed magma, thus may retain its primary Hf isotopic signature acquired from the magma and survive post-crystallization thermal disturbances (Kinny and Maas, 2003; Zheng et al., 2007).

Magma mixing process has long been considered as an important mechanism in producing granitoids. When small volumes of mafic magma injects into a felsic magma chamber, the mafic magma would cool rapidly and become more viscous to form discrete magma globules (Vernon, 1984; Griffin et al., 2002; Barbarin, 2005; Yang et al., 2007). In the case of the Ulaan Uul batholith and

Table 1

Major oxides (wt.%) and trace element (ppm) concentrations of the Ulaan Uul batholith and associated Mafic enclaves in the Bayankhongor area, central Mongolia.

Sample	Ulaan Uul batholith										MME	
	MG11-89-9	MG11-89-10	MG11-89-11	MG11-89-12	MG11-89-13	MG11-89-14	MG11-89-15	MG11-89-16	MG11-89-17	MG11-89-18	MG11-89-1	MG11-89-2
Major oxides (wt.%)												
SiO_2	73.3	67.3	69.5	68.0	70.2	68.8	70.1	75.4	69.3	66.0	54.1	55.9
TiO_2	0.23	0.64	0.31	0.51	0.42	0.44	0.45	0.27	0.40	0.64	1.56	1.39
Al_2O_3	14.1	15.4	15.9	15.9	15.5	15.2	15.1	12.3	15.9	16.3	18.0	18.1
$Fe_2O_3^T$	1.60	3.74	1.97	2.89	2.57	3.54	2.73	1.98	2.17	3.59	8.19	7.51
MnO	0.02	0.06	0.03	0.04	0.04	0.04	0.04	0.03	0.04	0.06	0.17	0.15
MgO	0.55	1.47	0.60	1.02	0.99	0.90	1.10	0.59	0.95	1.45	3.56	3.25
CaO	0.75	2.04	0.71	1.37	0.87	0.98	0.86	0.82	0.80	1.63	5.40	4.73
Na_2O	3.29	4.35	3.74	4.01	4.35	4.02	4.46	3.06	3.96	3.89	4.81	4.87
K_2O	5.13	2.94	6.23	4.72	4.18	4.59	3.78	4.07	5.31	4.79	2.13	2.33
P_2O_5	0.05	0.22	0.08	0.17	0.15	0.11	0.15	0.07	0.12	0.21	0.48	0.42
L.O.I	0.87	1.63	0.81	1.18	0.65	1.22	1.11	1.27	0.85	1.27	1.39	1.18
Total	99.9	99.8	99.9	99.9	99.8	99.8	99.6	99.9	99.8	99.8	99.8	99.8
Trace elements (ppm)												
Sc	0.58	4.71	0.66	1.08	1.50	1.16	2.94	0.73	1.25	3.93	17.3	15.0
Ti	1223	3127	1638	2634	2145	2363	2352	1443	2151	3324	8915	7711
V	27.4	41.3	27.0	38.7	31.3	52.8	33.1	29.8	30.7	48.3	116	104
Cr	7.93	8.33	7.27	10.0	9.32	8.70	7.16	8.34	9.92	13.6	35.8	30.5
Mn	177	425	220	316	304	314	330	197	257	438	1294	1145
Co	2.99	6.82	2.84	4.90	4.85	4.76	4.63	3.22	4.17	7.25	17.6	16.1
Ni	1.58	3.88	1.74	2.10	2.87	2.25	2.70	1.64	2.04	5.69	22.2	18.1
Cu	2.25	4.37	1.98	2.78	2.47	2.68	2.09	1.79	2.14	6.38	9.36	8.23
Zn	23.7	50.6	26.6	40.6	37.8	42.9	40.4	30.2	32.6	53.5	122	117
Ga	14.2	18.8	15.6	17.4	16.7	18.0	17.0	13.1	16.4	19.1	26.1	26.2
Ge	1.10	1.32	1.20	1.30	1.16	1.54	1.11	1.25	1.12	1.47	1.92	1.99
Rb	105	68.8	130	97.9	93.5	92.0	91.3	80.7	110	107	94.2	104
Sr	614	742	475	689	532	554	440	519	584	736	784	791
Y	8.14	22.7	11.7	19.3	12.9	17.2	14.5	7.98	9.07	22.4	42.6	34.9
Zr	170	250	207	213	177	280	167	234	140	215	134	150
Nb	5.17	18.8	10.3	16.6	9.67	12.4	12.0	6.23	9.66	18.6	36.6	33.5
Cs	0.50	1.31	0.35	0.72	0.52	0.38	0.40	0.46	0.48	1.53	1.38	1.55
Ba	2375	1189	2544	1984	1655	1955	1240	1876	2354	2056	475	425
La	62.4	60.7	46.1	46.7	40.1	131	34.1	71.7	39.9	39.9	41.7	38.9
Ce	107	120	87.5	101	76.7	238	71.5	123	70.0	94.8	117	109
Pr	10.2	14.3	9.74	12.6	8.73	23.9	8.69	12.1	7.87	11.9	17.6	15.9
Nd	30.6	51.8	32.8	44.9	29.8	73.2	31.2	36.2	26.8	44.4	73.3	63.8
Sm	3.47	8.48	4.78	7.49	4.780	8.70	5.37	4.08	4.04	7.81	14.3	11.9
Eu	0.43	1.56	0.78	1.24	0.83	1.22	1.00	0.54	0.79	1.43	3.02	2.52
Gd	1.89	6.05	3.06	5.26	3.31	4.30	3.72	2.01	2.57	5.48	11.0	9.00
Tb	0.29	0.93	0.46	0.77	0.51	0.73	0.57	0.32	0.39	0.84	1.66	1.34
Dy	1.58	4.86	2.33	4.05	2.68	3.71	3.13	1.67	2.04	4.64	8.89	7.13
Ho	0.30	0.90	0.45	0.75	0.51	0.68	0.59	0.31	0.37	0.88	1.68	1.36
Er	0.80	2.32	1.15	1.93	1.26	1.70	1.49	0.83	0.92	2.17	4.27	3.48
Tm	0.12	0.33	0.16	0.27	0.19	0.24	0.21	0.12	0.13	0.31	0.60	0.49
Yb	0.78	2.11	1.09	1.72	1.16	1.54	1.32	0.79	0.82	1.94	3.83	3.22
Lu	0.12	0.30	0.16	0.24	0.17	0.22	0.19	0.13	0.12	0.28	0.53	0.46
Hf	3.75	5.82	4.88	4.98	4.32	6.29	4.16	5.16	3.48	4.95	3.25	3.65
Ta	0.53	2.21	1.10	1.95	1.10	1.40	1.29	0.64	1.03	1.86	3.38	3.43
Pb	18.0	11.4	15.2	17.4	15.1	15.9	10.9	15.5	16.3	15.7	9.56	9.27
Th	8.28	7.91	6.13	7.36	5.81	15.2	4.73	8.58	4.71	5.81	6.17	5.85
U	0.35	0.91	0.58	0.85	0.86	0.60	1.01	0.41	0.65	0.86	1.33	1.36
Mg#	44.4	47.8	41.4	45.2	47.4	37.1	48.5	41.1	50.4	48.5	50.3	50.2

Table 1 (*continued*)

Sample	MME					
	MG11-89-3	MG11-89-4	MG11-89-5	MG11-89-6	MG11-89-7	MG11-89-8
Major oxides (wt.%)						
SiO_2	67.5	55.2	52.1	53.5	52.8	64.6
TiO_2	0.66	1.38	1.56	1.47	1.53	0.71
Al_2O_3	14.7	18.3	19.1	18.2	18.9	17.0
$Fe_2O_3^T$	4.87	7.46	8.50	8.00	8.35	4.03
MnO	0.06	0.17	0.17	0.12	0.15	0.07
MgO	1.31	3.06	3.74	4.03	3.71	1.42
CaO	3.08	5.57	5.14	5.83	5.71	2.64
Na_2O	4.10	5.02	4.83	4.50	4.73	4.33
K_2O	1.65	2.05	2.65	2.40	2.53	3.98
P_2O_5	0.20	0.37	0.41	0.39	0.40	0.25
L.O.I	1.71	1.21	1.60	1.31	0.86	0.78
Total	99.9	99.8	99.8	99.8	99.8	99.8
Trace elements (ppm)						
Sc	1.26	18.4	16.5	11.6	11.7	3.16
Ti	3586	7614	8288	7831	8059	4237
V	86.9	105	119	136	129	56.3
Cr	15.1	22.0	23.1	35.5	19.5	17.2
Mn	445	1200	1257	892	1120	538
Co	8.37	17.9	21.6	23.4	21.1	8.45
Ni	5.09	12.8	16.1	23.8	16.1	6.81
Cu	5.02	61.9	45.3	26.5	15.7	3.07
Zn	61.3	107	127	93.6	113	66
Ga	19.4	26.2	26.8	22.8	25.0	22.7
Ge	1.27	2.13	1.81	1.48	1.49	1.69
Rb	65.2	49.9	118	78.1	111	123
Sr	791	772	854	907	794	854
Y	9.12	64.5	40.6	13.6	18.6	23.7
Zr	180	224	184	159	189	269
Nb	10.3	52.5	34.9	10.5	15.6	21.7
Cs	0.89	1.00	1.60	1.09	1.53	1.67
Ba	435	423	592	777	518	1547
La	65.5	41.1	39.0	32.5	33.0	63.2
Ce	113	123	109	61.7	69.7	123
Pr	11.6	20.6	16.5	7.22	9.20	14.6
Nd	35.1	89.2	67.4	28.6	36.4	51.1
Sm	3.87	18.8	13.0	5.30	6.45	8.22
Eu	0.80	3.59	2.68	1.52	1.63	1.62
Gd	1.95	15.2	10.0	4.26	5.04	5.55
Tb	0.28	2.36	1.55	0.62	0.72	0.87
Dy	1.53	13.0	8.49	3.17	3.84	4.62
Ho	0.32	2.54	1.63	0.60	0.74	0.89
Er	0.91	6.64	4.09	1.37	1.89	2.29
Tm	0.15	0.96	0.60	0.19	0.26	0.33
Yb	1.19	6.17	3.86	1.16	1.63	2.11
Lu	0.21	0.86	0.54	0.17	0.25	0.30
Hf	7.34	5.72	4.23	3.74	4.32	6.16
Ta	0.69	6.54	3.61	0.43	0.94	2.14
Pb	9.19	10.8	9.67	9.19	13.7	16.5
Th	8.33	7.60	4.77	3.67	2.63	9.19
U	0.86	1.79	1.22	1.00	0.71	1.51
$Mg^\#$	38.6	48.9	50.6	54.0	50.8	45.1

$Mg^\# = 100 * Mg/(Mg + Fe^{2+})$, assuming $Fe^{2+}/Fe^{total} = 0.85$; LOI = loss of ignition; $Fe_2O_3^T$ = total Fe oxides as Fe_2O_3.

Fig. 6. Petrochemical diagrams of the host granite and MMEs. (a) Total alkali–silica (TAS) diagram (Le Bas et al., 1986); (b) SiO₂–K₂O diagram (Peccerillo and Taylor, 1976); (c) ANK–ACNK diagram (Maniar and Piccoli, 1989). Data for the high Ba–Sr appinites and granitoids in the Scottish Caledonides from Fowler and Henney (1996) and Fowler et al. (2001, 2008).

associated MMEs, there are some characteristics in support of magma mixing. For example, some MMEs within the Ulaan Uul batholith contain large K-feldspar phenocrysts, suggesting a non-consolidation state which allows physical transfer of crystals from the host felsic magma into the mafic magma (Fig. 3a) (Waight et al., 2000; Perugini et al., 2003). In addition, the finer grained texture of the MMEs was caused by the undercooling of a hot mafic magma in a relatively cool, felsic magma (Vernon, 1984). As a

mineral crystallized in the early stage of magma, zircon has high Lu–Hf closure temperature (>800 °C) and hence can record primitive isotopic signatures of the magmatic components and subsequent isotopic variations during the mixing process (Cherniak and Waston, 2001; Griffin et al., 2002; Kemp and Hawkesworth, 2006; Yang et al., 2007; Li et al., 2009). Most zircons from the MMEs have positive $\varepsilon Hf(t)$ values (0.7–2.6) with single-stage Hf model ages of 1.05–1.12 Ga, while others have negative $\varepsilon Hf(t)$ values (−0.75 to −3.5) with two-stage Hf model ages of 1.51–1.72 Ga. In contrast, most of the zircons from the host granite have negative $\varepsilon Hf(t)$ values (−0.63 to −11.9) with two-stage Hf model ages of 1.54–2.25 Ga, and only two spots posses positive $\varepsilon Hf(t)$ values of 0.12 and 1.4 with single-stage Hf model ages of 1.13 and 1.08 Ga, respectively (Fig. 10). The distinct Hf isotopic compositions of zircons from the MMEs and host granite does not reflect a simple, cogenetic evolution through closed-system fractionation. Rather, the different Hf isotopic compositions of the zircons suggest that the MMEs and their host granite were probably derived from different sources, and that magma mixing/mingling process is the most likely regime to form the Ulaan Uul batholith. Such a mixing mechanism can be further testified by the hyperbolic curves in diagrams involving two ratios of incompatible elements (Langmuir et al., 1978). In the plot of Zr/Sm vs. Th/La, rocks from the Ulaan Uul batholith and associated MMEs define a characteristic hyperbolic mixing line (Fig. 12a), consistent with a two-component mixing process. In addition, the binary diagrams of $^{143}Nd/^{144}Nd$ vs. $^{147}Sm/^{144}Nd$ and Rb/Sr vs. $^{87}Sr/^{86}Sr$ (Fig. 12b and c) confirm that the magma mixing process is a valid mechanism in the genesis of the host rocks.

5.2. Source nature of the MMEs and host granite

The MMEs possess low SiO₂ (mostly <56 wt.%) contents, high Mg# (up to 55) as well as relatively high V (up to 136 ppm) and Cr (up to 36 ppm) concentrations, suggesting that a mantle component played a prominent role in their genesis (Wilson, 1989; Rudnick and Gao, 2003). Several MME samples with high Mg# (50–55) may represent more primitive magmatic components, and display enriched Sr–Nd isotopic compositions (initial $^{87}Sr/^{86}Sr$ = 0.7062 to 0.7063; $\varepsilon Nd(t)$ = −1.6 to −1.7). The Sr–Nd isotopic compositions of the MMEs are significantly different from those of the Bayankhongor ophiolites that are thought to derive from a depleted asthenospheric mantle (Fig. 9a) (Jian et al., 2010). Furthermore, MME zircons with positive $\varepsilon Hf(t)$ values show single-stage Hf model ages (1.05–1.12 Ga) that are much older than the zircon U–Pb ages of 547 Ma, implying a late Mesoproterozoic lithospheric mantle source. Recently, a Mesoproterozoic lithospheric mantle of the Hangay zone was proposed based on the Mesoproterozoic Nd model ages (1.4–1.1 Ga) of granitoids (Kovalenko et al., 2004) and T_{RD} model ages (1.5–1.3 Ga and 1.0 Ga) for the sulfides from spinel peridotite xenoliths (Wang et al., 2013). The above evidence indicates that the MMEs were likely derived from partial melting of Mesoproterozoic lithospheric mantle that reworked at the early Cambrian.

Rocks from the host granite exhibit high SiO₂, low MgO, Cr and Ni contents, and enriched Sr–Nd–Hf isotopic compositions, reflecting a crustal origin. Compositional diversity of crustally derived melts strongly depends on source compositions and variable melting conditions (Beard and Lofgren, 1991; Rapp et al., 1991; Patiño Douce and Beard, 1995; Thompson and Connolly, 1995). To identify the possible source, it is necessary to compare the chemical and isotopic compositions of the host granite with those of crustal rocks in the surrounding areas. The Archean to Paleoproterozoic basement rocks in the Baydrag block are characterized by far more negative $\varepsilon Nd(t)$ values (−14.52 to −33.24, calculated at 547 Ma) (Kozakov et al., 1997) than those of the host granite. Compared
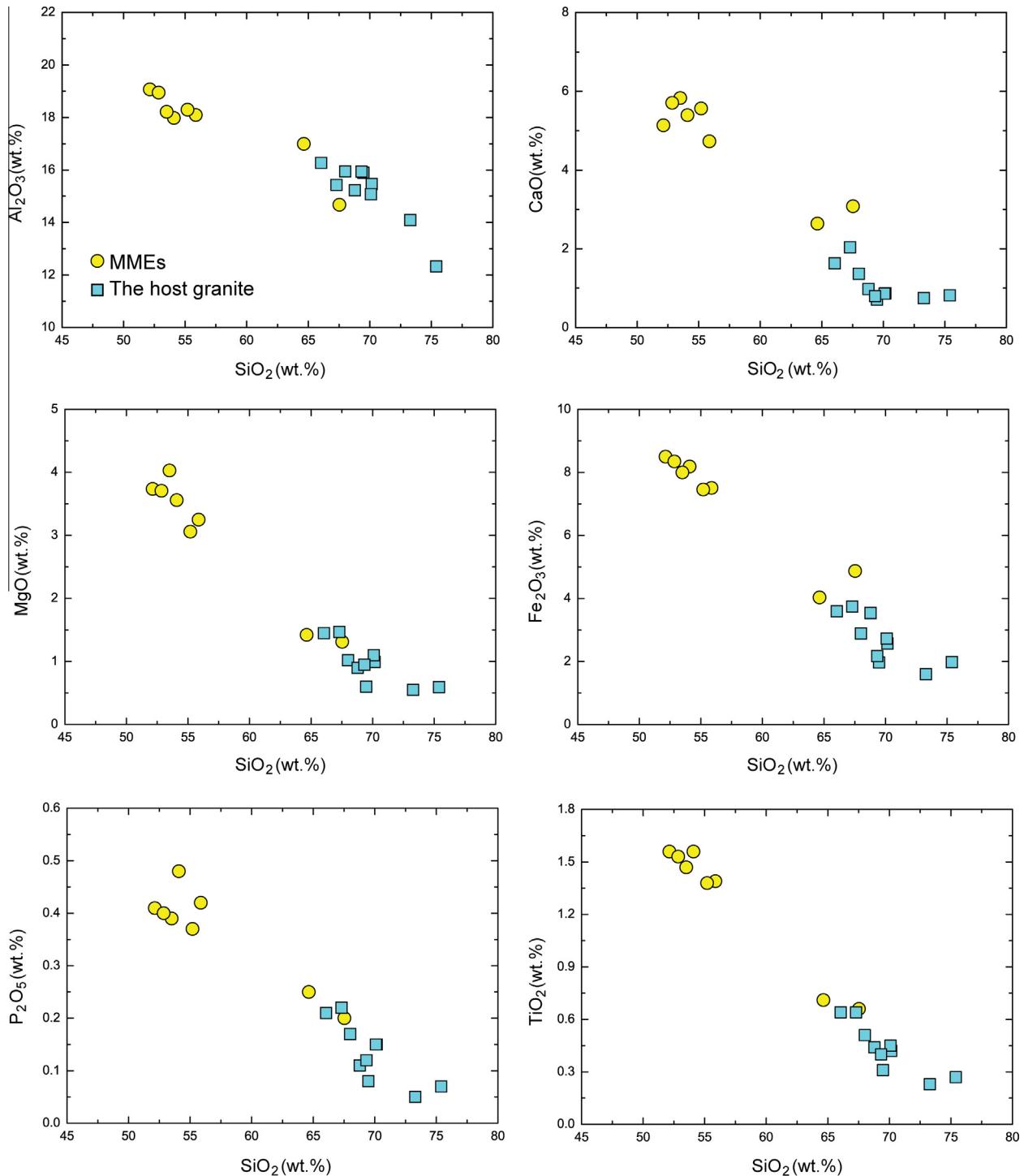
Fig. 7. Binary diagrams of oxides vs. SiO_2 for the host granite and MMEs.

with the basement rocks, the Neoproterozoic Burd Gol accretionary complex that derived from the Baydrag block displays less negative initial $\varepsilon Nd(t)$ values (-11.5 to -16.1) (Kovalenko et al., 2005). However, both the Archean to Paleoproterozoic basement rocks and the Neoproterozoic Burd Gol accretionary complex cannot be the possible protolith due to their strongly negative $\varepsilon Nd(t)$ (Fig. 9a and b). In contrast, sedimentary rocks from the Bayankhongor zone and the Dzag zone exhibit slightly negative $\varepsilon Nd(t)$ and young Nd model ages, which are similar to those of the host granite. For instance, phyllites from the Huluut Bulag mélange gave initial $\varepsilon Nd(t)$ values of -4.2 to -3.2 with Nd modal ages of 1.5–

1.7 Ga (Fig. 7b) (Kovalenko et al., 2005). Pelitic schists of the Dzag zone yielded initial $\varepsilon Nd(t)$ values of -3.1 to -3.7 with Nd model ages of 1.6–1.5 Ga (Jahn et al., 2004; Kovalenko et al., 2005). Therefore, we suggest that the felsic pelite is a potential candidate for the source of the host granite. This conclusion is further supported by whole-rock geochemistry. Jung and Pfänder (2007) proposed that CaO/Na_2O ratios of crust-derived melts strongly depend on the source compositions and can be used to distinguish between pelite-derived melts ($CaO/Na_2O < 0.5$) and melts derived from greywackes or igneous rocks (CaO/Na_2O: 0.3–1.5). Samples from the host granite have low CaO/Na_2O ratios (0.19–0.49, mostly
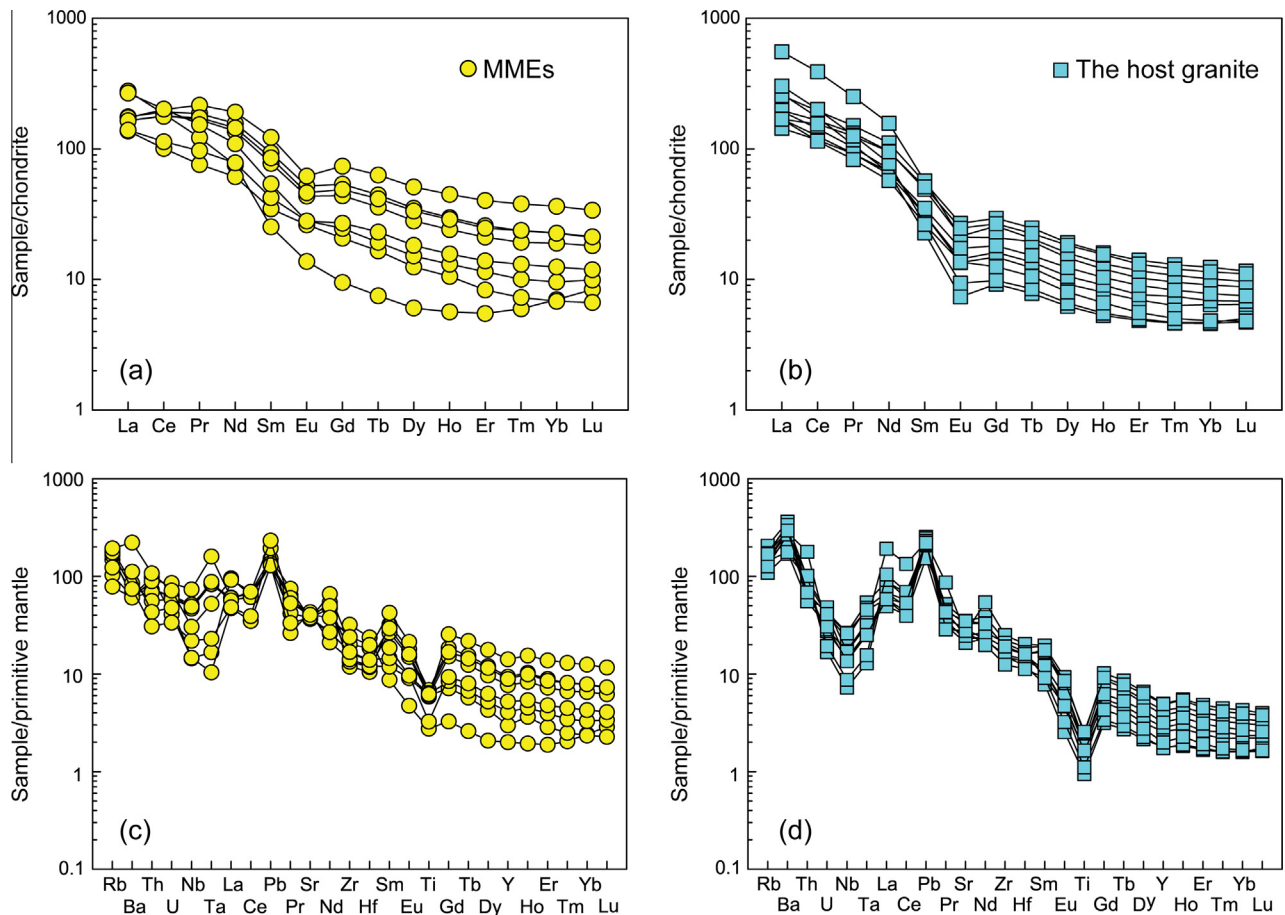
Fig. 8. Chondrite-normalized REE patterns (a and b) and primitive mantle-normalized multi-element patterns (c and d) for the host granite and MMEs. Normalizing values from Sun and McDonough (1989).

Table 2
Sm–Nd and Rb–Sr isotopic analytical results of the Ulaan Uul batholith and associated MMEs in the Bayankhongor area, central Mongolia.

Sample	Rb (ppm)	Sr (ppm)	$^{87}Rb/^{86}Sr$	$^{87}Sr/^{86}Sr$	$(^{87}Sr/^{86}Sr)i$	Sm (ppm)	Nd (ppm)	$^{147}Sm/^{144}Nd$	$^{143}Nd/^{144}Nd$	$(^{143}Nd/^{144}Nd)i$	$T_{DM1}(Ga)$	$T_{DM2}(Ga)$	$\varepsilon Nd(t)$
MG11-89-2	104	791	0.382	0.709188	0.706213	11.9	63.8	0.1124	0.512256	0.511854	1.35	1.41	−1.6
MG11-89-3	65.2	791	0.239	0.708483	0.706621	3.87	35.1	0.0667	0.512070	0.511831	1.12	1.44	−2.0
MG11-89-5	119	854	0.402	0.709466	0.706335	13.0	67.4	0.1168	0.512264	0.511846	1.39	1.42	−1.7
MG11-89-8	123	854	0.416	0.709255	0.706009	8.22	51.1	0.0972	0.512174	0.511826	1.28	1.45	−2.1
MG11-89-9	106	614	0.497	0.709769	0.705894	3.47	30.6	0.0687	0.512074	0.511827	1.13	1.45	−2.1
MG11-89-14	92.0	554	0.480	0.710208	0.706463	8.70	73.2	0.0718	0.512097	0.511840	1.13	1.43	−1.8
MG11-89-15	91.3	441	0.600	0.711120	0.706443	5.37	31.3	0.1038	0.512212	0.511840	1.30	1.43	−1.8
MG11-89-18	108	736	0.423	0.709353	0.706052	7.81	44.4	0.1062	0.512216	0.511835	1.33	1.44	−1.9

<0.3), suggesting a pelite-dominated origin. In addition, their high $Al_2O_3/(MgO + FeO^T)$ and low $CaO/(MgO + FeO^T)$ ratios also suggest a felsic pelite source (Fig. 13), because melts derived from metapelites possess higher $Al_2O_3/(MgO + FeO^T)$ but lower $CaO/(MgO + FeO^T)$ ratios than those from metabasalts and metagreywackes (Gerdes et al., 2002). Partial melting of felsic pelites needs a heat source, which can be provided by the underplating of a basaltic magma (represented by the MMEs). Thus, intrusion of Mesoproterozoic SCLM-derived basaltic magma created a thermal anomaly to trigger partial melting of the felsic pelites and subsequent mixing between the mantle- and pelite-derived melts resulted in the formation of the host granite.

5.3. Implication for the petrogenesis of high Ba–Sr granitoids

The Ulaan Uul batholith displays high Ba (1189–2544 ppm), Sr (440–745 ppm), K/Rb (354–418), but low Rb/Ba (<0.07), compara-

ble to those of typical high Ba–Sr granitoids (Fig. 11). High Ba–Sr granitoids share some common geochemical features: (1) high contents LILEs such as Ba, Sr and K_2O; (2) crust-like Sr–Nd–Hf–Pb–O isotopic compositions (Tarney and Jones, 1994; Fowler and Rollinson, 2012; Peng et al., 2013). To explain these features, an origin from partial melting of an enriched SCLM metasomatized by sedimentary melts and/or fluids via subduction was proposed (Qian et al., 2003; Fowler et al., 2001, 2008; Fowler and Rollinson, 2012; Jiang et al., 2012; Peng et al., 2013). Terrigenous sediments-derived melts or aqueous fluids could carry voluminous Ba and Sr (Plank and Langmuir, 1998; Kilian and Behrmann, 2003; Portnyagin et al., 2007), and transfer of these elements would result in enrichment of associated lithospheric mantle. Large volume of sediments eroded from the continents will deposit on ocean floor and significantly recycle into the mantle through subduction. Moreover, almost all of the high Ba–Sr granitic intrusions in the world are located on continental margins. Therefore, it is
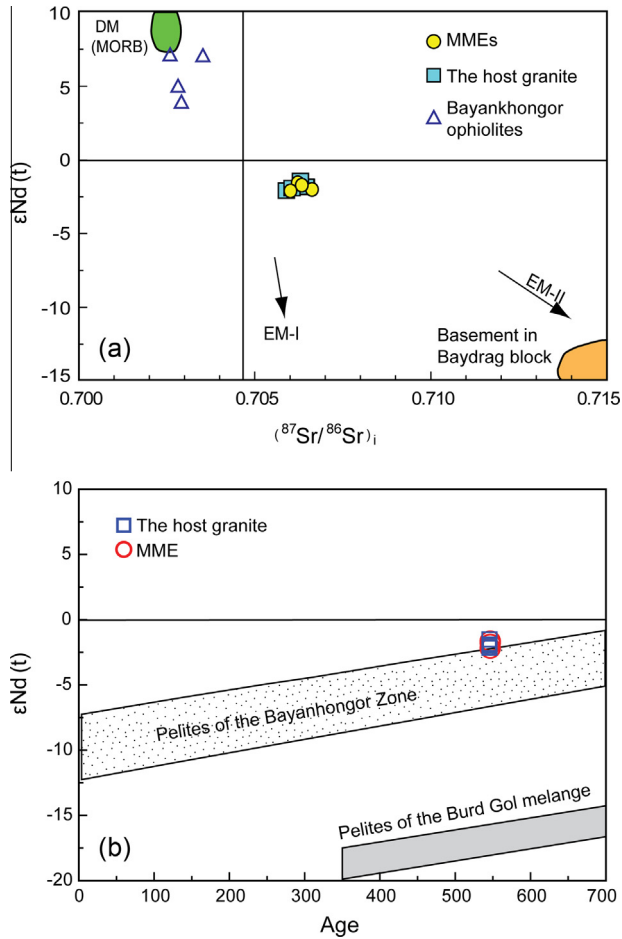
Fig. 9. (a) Diagram of $\varepsilon Nd(t)$ vs. $(^{87}Sr/^{86}Sr)_i$ for the host granite and associated MMEs (modified after Jahn et al., 2009); (b) $\varepsilon Nd(t)$ vs. U–Pb ages for zircons from the host granite and associated MMEs (modified after Kovalenko et al., 2005).

Fig. 10. Relative probability diagrams for $\varepsilon Hf(t)$ values of zircons from the host granite (a) and associated MMEs (b).

reasonable to infer that terrestrial materials can significantly recycle into the mantle source in the form of sediment-derived fluids and/or melts via subduction along the continental margins, and that interaction of terrestrial sediment-derived fluid or melt can give rise to an enriched lithospheric mantle. Subsequent low-degree partial melting of the metasomatized lithospheric mantle will produce melts with high Ba–Sr signatures.

Our petrogenetic model for the Ulaan Uul batholith, i.e., melts of sedimentary materials and subsequent mixing with mantle-derived magma may shed new lights on the origin of high Ba–Sr granitoids. Our geochemical data indicate that the high Ba–Sr batholith was not entirely derived from an enriched lithospheric mantle as other high Ba–Sr granitoids in the world. In fact, rocks from the high Ba–Sr Ulaan Uul batholith display more remarkable sedimentary signatures than those of the high Ba–Sr appinites and granitoids from the Scottish Caledonides, as suggested by their higher A/CNK and A/NK ratios (Fig. 6c). As discussed above, the newly accreted sediments in the Haluut Bulag mélange played an important role in the formation of the high Ba–Sr batholith. This model suggests that the high Ba–Sr signatures can be achieved not only by the recycle of terrigenous sediments in the mantle, but also by crust–mantle magma mixing process.

5.4. Geodynamic implication

Generally, high Ba–Sr granitoid rocks have been considered to be emplaced in a post-collisional extensional setting caused by
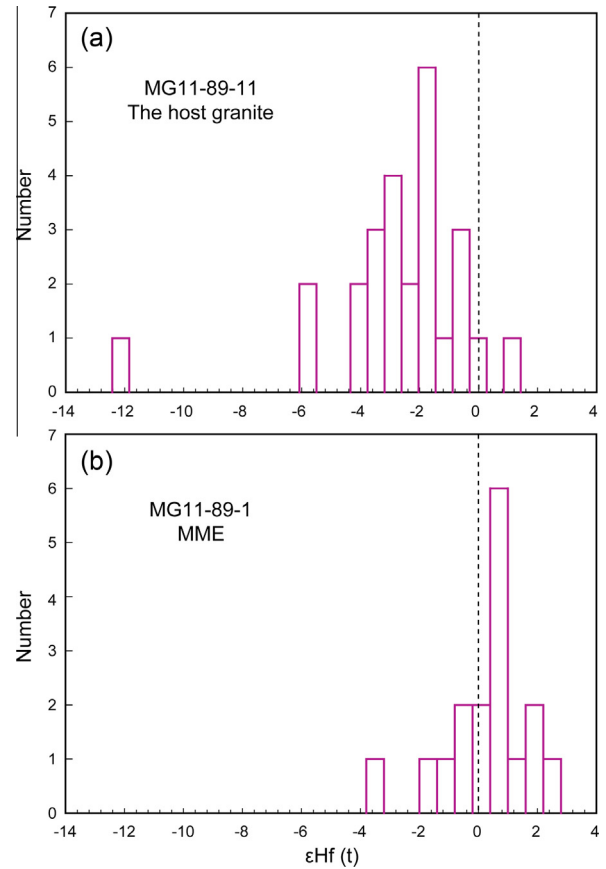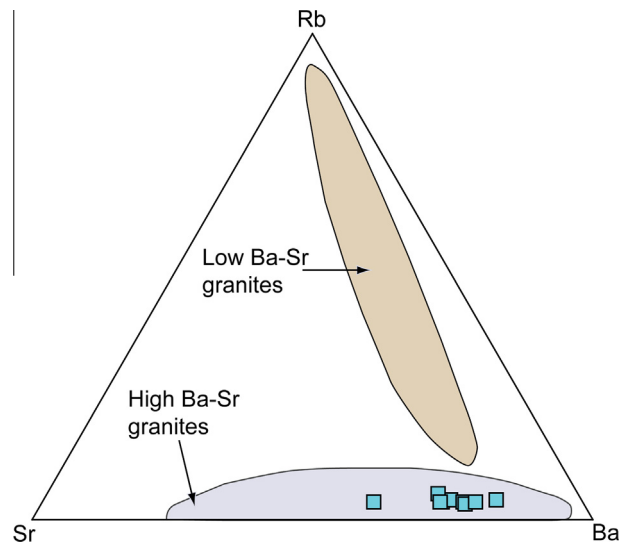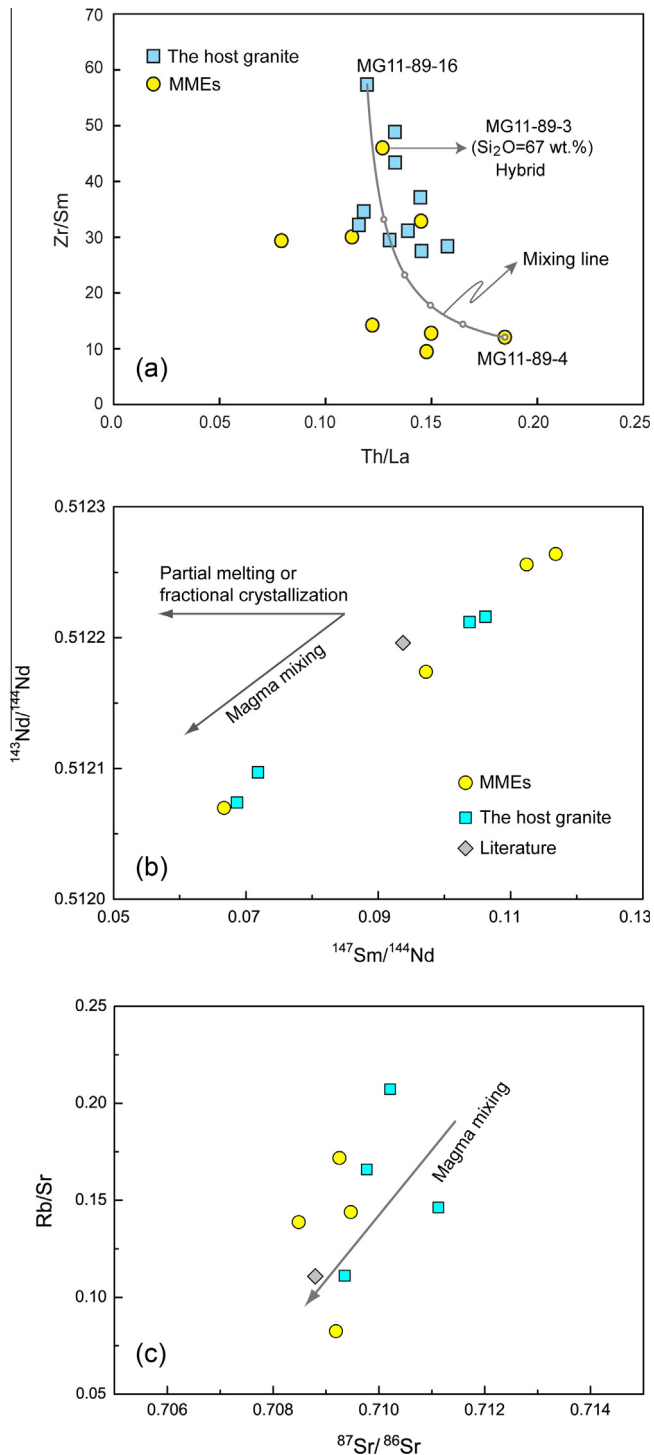

Fig. 11. Sr–Rb–Ba plot (modified after Tarney and Jones, 1994) for the host granite.
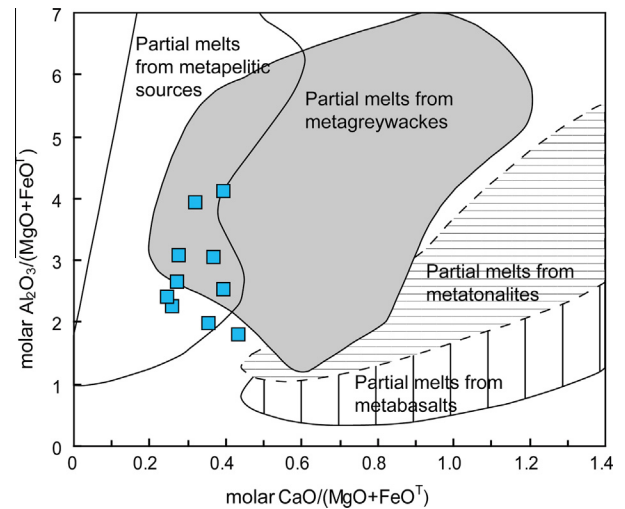
slab break-off or gravitational collapse (Qian et al., 2003; Fowler et al., 2001, 2008; Fowler and Rollinson, 2012; Ye et al., 2008; Heilimo et al., 2010). Recently, a subduction-related setting has been proposed to account for the formation of high Ba–Sr granitoids (González-Guillot et al., 2012; Peng et al., 2013; Cardona

Fig. 12. Selected geochemical variation diagrams for the host granite and MMEs. These variations strongly show that crust–mantle magma mixing takes place. (a) Th/La vs. Zr/Sm covariant diagram; (b) $^{143}Nd/^{144}Nd$ vs. $^{147}Nd/^{144}Nd$ and (c) Rb/Sr vs. $^{87}Sr/^{86}Sr$ diagrams.

Fig. 13. Molar $Al_2O_3/(MgO + FeO^T)$ vs. molar $CaO/(MgO + FeO^T)$ diagram for the host granite (after Gerdes et al., 2002).

Hangai microcontinent decrease in age from south to north (Buchan et al., 2002; Demoux et al., 2009; Kröner et al., 2011), suggesting that the subduction zone migrated northwards. In the early Neoproterozoic, the Burd Gol mélange developed on the northern margin of the Baydrag block, due to the subduction of the Bayankhongor oceanic lithosphere beneath the Baydrag block (Fig. 14a) (Demoux et al., 2009). Along with the sweep-back of the subducting Bayankhongor oceanic slab, the South Volcanic Belt and the Delb Khairkhan mélange formed on a southward–dipping subduction zone in the middle to late Neoproterozoic (Fig. 14b) (Dergunov et al., 1997). Meanwhile, the Bayankhongor alkaline lavas were built on the oceanic crust, and subsequently accreted to the Delb Khairkhan mélange (Fig. 14b and c).

Regional metamorphic and magmatic events also recorded the accretionary process of the intervening mélanges onto the Baydrag microcontinent. The Burd Gol mélange underwent Barrovian-type metamorphism with metamorphic grade increasing northwards (Buchan et al., 2001), and metamorphic white micas from a pelitic schist gave a K–Ar age of 699 ± 35 Ma reflecting an early-stage accretion of the Burd Gol mélange onto the Baydrag block (Teraoka et al., 1996). In addition, a biotite–garnet schist from the Burd Gol mélange yielded a biotite $^{40}Ar/^{39}Ar$ plateau age of 533 ± 3 Ma (Höck et al., 2000). This prolonged metamorphism probably reflects the punctuated southward accretion–collision. Recent zircon U–Pb dating results demonstrate that late Neoproterozoic to early Cambrian granitic magmatism was widespread in the Bayankhongor region (Buchan et al., 2002; Jahn et al., 2004; Kozakov et al., 2006, 2008; Demoux et al., 2009; Jian et al., 2010). Furthermore, it is found that the late Neoproterozoic (580–540 Ma) granitic intrusions are mainly distributed in the Baydrag block and Burd Gol mélange, whereas those of early Cambrian (540–510) are widespread in the whole region. This trend clearly reflects the northward migration of a subduction zone. For instance, two gneissic granites that intruded the Burd Gol mélange yielded zircon U–Pb ages of 579 and 560 Ma, respectively (Demoux et al., 2009). The Ulaan Uul batholith formed at 546 ± 3 Ma and was probably related to the roll-back of the subducted Bayankhongor oceanic lithosphere. In this scenario, a descending slab migrating backwards would induce upwelling of the deep asthenosphere and cause a thermal anomaly in the mantle wedge. Subsequent partial melting of the Mesoproterozoic SCLM and underplating basaltic magma gave rise to partial melting of overlying sedimentary materials (Fig. 14c).

et al., 2014). In conjunction with regional geology and magmatic evolutionary history, we suggest that formation of the Ulaan Uul batholith with high Ba–Sr signatures was not related to a post-collisional setting, but rather formed in a subduction-related setting.
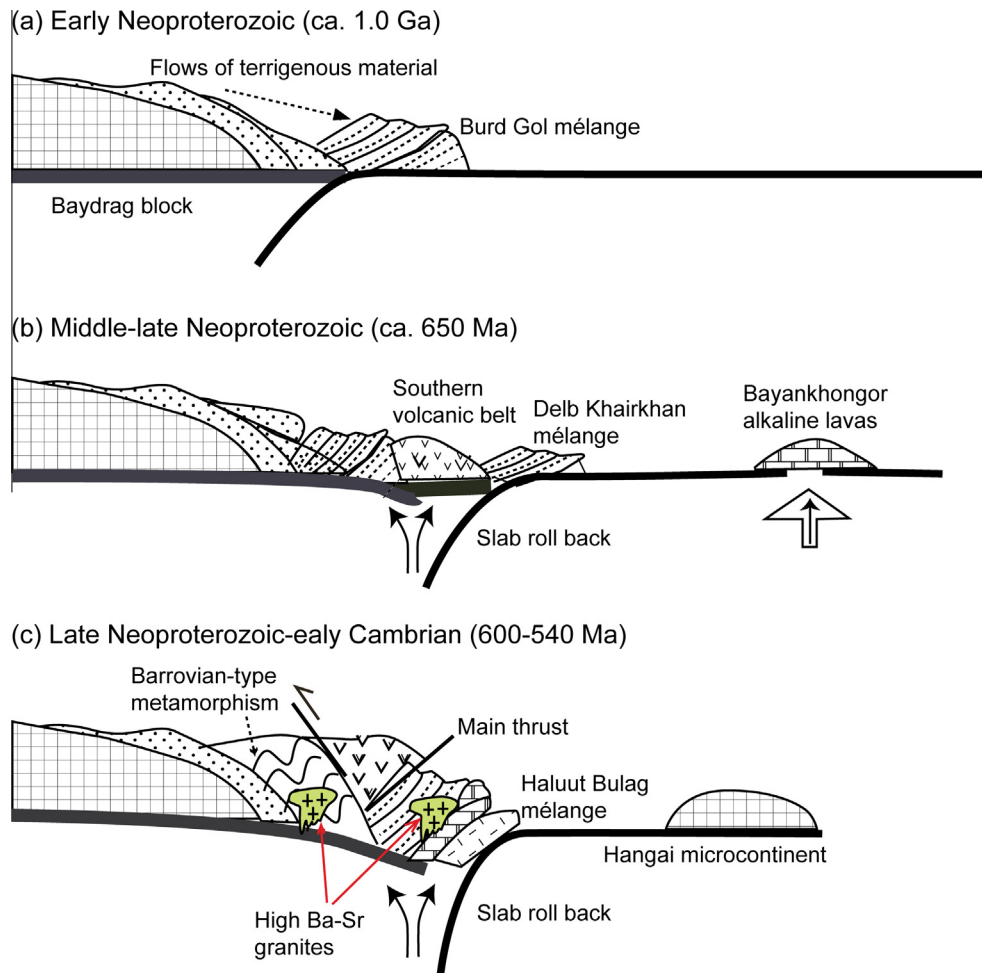
As described in Section 2.1, several tectonic terranes have been recognized in the Bayankhongor region. A striking feature is that the intervening mélanges between the Baydrag block and the

(a) Early Neoproterozoic (ca. 1.0 Ga)

(b) Middle-late Neoproterozoic (ca. 650 Ma)

(c) Late Neoproterozoic-ealy Cambrian (600-540 Ma)

Fig. 14. Schematic diagrams for the Neoproterozoic to early Cambrian tectonic evolution of the Bayankhongor area, central Mongolia. (a) Southward subduction of the Bayankhongor oceanic lithosphere and the formation of the Burd Gol mélange; (b) accretion of the Burd Gol mélange onto the Baydrag block and a new subduction zone developed on the northern margin of the Burd Gol mélange which account for the formation of the southern volcanic belt and the Delb Khairkhan mélange; (c) due to the roll-back of the Bayankhongor oceanic lithosphere, the Bayankhongor ophiolite was accreted onto the Burd Gol mélange by incorporation of two accretionary wedges (the Delb Khairkhan and Haluut Bulag mélange), and the high Ba–Sr granites were emplaced into the mélanges.

6. Conclusions

(1) LA–ICP–MS zircon U–Pb dating has illustrated that the ages of the host granite and MMEs are 546 ± 3 Ma and 547 ± 3 Ma, respectively, indicating that the mafic and felsic magmas were coeval.

(2) The petrographic observations and geochemical data indicate that the parental magma of the MMEs was derived from an enriched Mesoproterozoic SCLM. The host granite, classified as high Ba–Sr granitoids, was produced by partial melting of felsic pelites triggered by upwelling of lithospheric mantle-derived magma (represented by MME) and subsequent mixing of the mantle- and sediment-derived melts.

(3) Considering available regional tectonic and magmatic data, it can be concluded that the formation of the Ulaan Uul batholith and associated MMEs was related to an extensional setting, as a tectonic response to the roll-back of the subducted Bayankhongor oceanic lithosphere.

Appendix A. Supplementary material

Supplementary data associated with this article can be found, in the online version, at http://dx.doi.org/10.1016/j.jseaes.2014.11.029.

References

Badarch, G., Cunningham, W.D., Windley, B.F., 2002. A new terrane subdivision for Mongolia: implications for the Phanerozoic crustal growth of Central Asia. J. Asian Earth Sci. 21, 87–104.

Barbarin, B., 2005. Mafic magmatic enclaves and mafic rocks associated with some granitoids of the central Sierra Nevada batholith, California: nature, origin, and relations with the hosts. Lithos 80, 155–177.

Beard, J.S., Lofgren, G.E., 1991. Dehydration melting and water-saturated melting of basaltic and andesitic greenstones and amphibolites at 1, 3, and 6.9 kb. J. Petrol. 32, 365–401.

Blichert-Toft, J., Albarede, F., 1997. The Lu–Hf geochemistry of chondrites and the evolution of the mantle–crust system. Earth Planet. Sci. Lett. 148, 243–258.

Bruand, E., Storey, C., Fowler, M., 2014. Accessory mineral chemistry of high Ba–Sr granites from northern Scotland: constraints on petrogenesis and records of whole-rock signature. J. Petrol. 55, 1619–1651.

Buchan, C., Cunningham, D., Windley, B.F., Tomurhuu, D., 2001. Structure and lithological characteristics of the Bayankhongor ophiolite zone, central Mongolia. J. Geol. Soc. London 158, 445–460.

Buchan, C., Pfäder, J., Kröner, A., Brewer, T.S., Tomurtogoo, O., Tomurhuu, D., Cunningham, D., Windley, B.F., 2002. Timing of accretion and collisional deformation in the Central Asian Orogenic Belt: implications of granite geochronology in the Bayankhongor Ophiolite Zone. Chem. Geol. 192, 23–45.

Cardona, A., Weber, M., Valencia, V., Bustamante, C., Montes, C., Cordani, U., Muñoz, C.M., 2014. Geochronology and geochemistry of the Parashi granitoid, NE Colombia: tectonic implication of short-lived Early Eocene plutonism along the SE Caribbean margin. J. S. Am. Earth Sci. 50, 75–92.

Chappell, B.W., White, A.J.R., 1992. I- and S-type granites in the Lachlan Fold Belt. Trans. R. Soc. Edinburgh: Earth Sci. 83, 1–26.

Cherniak, D.J., Waston, E.B., 2001. Pb diffusion in zircon. Chem. Geol. 172 (1), 5–24.

Choi, S.G., Rajesh, V.J., Seo, J., Park, J.W., Oh, C.W., Pak, S.J., Kim, S.W., 2009. Petrology, geochronology and tectonic implications of Mesozoic high Ba–Sr granites in the Haemi area, Hongseong Belt, South Korea. Island Arc 18, 266–281.

Dahlquist, J.A., 2002. Mafic microgranular enclaves: early segregation from metaluminous magma (Sierra de Chepes), Pampean Ranges, NW Argentina. J. S. Am. Earth Sci. 15 (6), 643–655.

Demoux, D., Kröner, A., Badarch, G., Jian, P., Tomurhuu, D., Michael, T.D.W., 2009. Geochronological constraints on Cambrian accretion-related magmatism in central Mongolia: evidence from the Bayankhongor and Baydrag terrains. J. Geol. 117, 377–397.

Dergunov, A.B., Ryantsev, A.V., Luneva, O.I., Rikhter, A.V., 1997. Structure and Geological History of the Bayan-Khongor Zone, central Mongolia. Geotectonics 31 (2), 132–140.

Didier, J., Barbarin, B., 1991. Enclaves and Granite Petrology, Developments in Petrology. Elsevier, Amsterdam, pp. 1–625.

Donaire, T., Pascual, E., Pin, C., Duthou, J.L., 2005. Microgranular enclaves as evidence of rapid cooling in granitoid rocks: the case of the Los Pedroches granodiorite, Iberian Massif, Spain. Contrib. Miner. Petrol. 149 (3), 247–265.

Eklund, O., Konopelko, D., Rutanen, H., Fröjdö, S., Shebanov, A.D., 1998. 1.8 Ga Svecofennian post-collisional shoshonitic magmatism in the Fennoscandian shield. Lithos 45, 87–108.

Fowler, M.B., Henney, P.J., 1996. Mixed Caledonian appinite magmas: implications for lamprophyre fractionation and high Ba–Sr granite genesis. Contrib. Miner. Petrol. 126, 199–215.

Fowler, M.B., Rollinson, H., 2012. Phanerozoic sanukitoids from Caledonian Scotland: implications for Archean subduction. Geology 40 (12), 1079–1082.

Fowler, M.B., Henney, P.J., Darbyshire, D.P.F., Greenwood, P.B., 2001. Petrogenesis of high Ba–Sr granites: the Rogart pluton, Sutherland. J. Geol. Soc. London 158, 521–534.

Fowler, M.B., Kocks, H., Darbyshire, D.P.F., Greenwood, P.B., 2008. Petrogenesis of high Ba–Sr plutons from the Northern Highlands Terrane of the British Caledonian Province. Lithos 105, 129–148.

Gerdes, A., Montero, P., Bea, F., Fershater, G., 2002. Peraluminous granites frequently with mantle-like isotope compositions: the continental-type Murzinka and Dzhabyk batholiths of the eastern Urals. Int. J. Earth Sci. 91, 3–19.

González-Guillot, M., Prezzi, C., Acevedo, R.D., Escayola, M., 2012. A comparative study of two rear-arc plutons and implications for the Fuegian Andes tectonic evolution: mount Kranck Pluton and Jeu-Jepén Monzonite, Argentina. J. S. Am. Earth Sci. 38, 71–88.

Griffin, W.L., Pearson, N.J., Elusive, E., Jackson, S.E., van Achtenberg, E., O'Reilly, S.Y., She, S.R., 2000. The Hf isotope composition of carbonic mantle: LAM–MC–ICPMS analysis of zircon megacrysts in kimberlites. Geochim. Cosmochim. Acta 64, 133–147.

Griffin, W.L., Wang, X., Jackson, S.E., Pearson, N.J., O'Reilly, S.Y., 2002. Zircon geochemistry and magma mixing, SE China: in situ analysis of Hf isotopes, Tonglu and Pingtan igneous complexes. Lithos 61, 237–269.

Heilimo, E., Halla, J., Hölttä, P., 2010. Discrimination and origin of the sanukitoid series: geochemical constraints from the Neoarchean western Karelian Province (Finland). Lithos 115 (1), 27–39.

Höck, V., Frank, W., Hejl, E., Furtmueller, G., 2000. Petrology and cooling history of the Mt. Ushgoeg Range (central Mongolia). In: Badarch, G., Jahn, B.M. (Eds.), IGCP-420 Continental Growth in the Phanerozoic: Evidence from Central Asia. Second Workshop, Abstracts and Excursion Guidebook, Ulaanbaatar, Mongolia. Geosciences Rennes, Hors Série, vol. 2, pp. 35–37.

Jahn, B.M., Wu, F.Y., Chen, B., 2000. Massive granitoid generation in Central Asia: Nd isotope evidence and implication for continental growth in the Phanerozoic. Episodes 23, 82–92.

Jahn, B.M., Capdevila, R., Liu, D.Y., Vernon, A., Badarch, G., 2004. Sources of Phanerozoic granitoids in the transect Bayankhongor-Ulaan Baatar, Mongolia: geochemical and Nd isotopic evidence, and implications for Phanerozoic crustal growth. J. Asian Earth Sci. 23, 629–653.

Jahn, B.M., Litvinovsky, B.A., Zanvilevich, A.N., Reichow, M., 2009. Peralkaline granitoid magmatism in the Mongolian-Transbaikalian Belt: evolution, petrogenesis and tectonic significance. Lithos 113 (3), 521–539.

Jian, P., Kröner, A., Windley, B.F., Shi, Y.R., Zhang, F.Q., Miao, L.C., Tomurhuu, D., Zhang, W., Liu, D.Y., 2010. Zircon ages of the Bayankhongor ophiolite mélange and associated rocks: time constraints on Neoproterozoic to Cambrian accretionary and collisional orogenesis in central Mongolia. Precambr. Res. 177 (1), 162–180.

Jiang, Y.D., Sun, M., Kröner, A., Tumurkhuu, D., Long, X.P., Zhao, G.C., Yuan, C., Xiao, W.J., 2012. The high-grade Tseel Terrane in SW Mongolia: an Early Paleozoic arc system or a Precambrian sliver? Lithos 142, 95–115.

Jung, S., Pfänder, J.A., 2007. Source composition and melting temperatures of orogenic granitoids: constraints from CaO/Na₂O, Al₂O₃/TiO₂ and accessory mineral saturation thermometry. Eur. J. Mineral. 19, 859–870.

Karsli, O., Chen, B., Aydin, F., Sen, C., 2007. Geochemical and Sr–Nd–Pb isotopic compositions of the Eocene Dölek and Sariçiçek Plutons, Eastern Turkey: implications for magma interaction in the genesis of high-K calc-alkaline granitoids in a post-collision extensional setting. Lithos 98, 67–96.

Kemp, A.I.S., Hawkesworth, C.J., 2006. Using hafnium and oxygen isotopes in zircons to unravel the record of crustal evolution. Chem. Geol. 226, 144–162.

Kemp, A.I.S., Wormald, R.J., Whitehouse, M.J., Price, R.C., 2005. Hf isotopes in zircon reveal contrasting sources and crystallization histories for alkaline to peralkaline granites of Temora, southeastern Australia. Geology 33, 797–800.

Kemp, A.I.S., Hawkesworth, C.J., Foster, G.L., Paterson, B.A., Woodhead, J.D., Hergt, J.M., Gray, C.M., Whitehouse, M.J., 2007. Magmatic and crustal differentiation history of granitic rocks from Hf–O isotopes in zircon. Science 315 (5814), 980–983.

Khain, E.V., Bibikova, E.V., Salnikova, E.B., Kröner, A., Gibsher, A.S., Didenko, A.N., Degtyarev, K.E., Fedotova, A.A., 2003. The Palaeo-Asian ocean in the Neoproterozoic and early Palaeozoic: new geochronologic data and palaeotectonic reconstructions. Precambr. Res. 122, 329–358.

Kilian, R., Behrmann, J.H., 2003. Geochemical constraints on the sources of Southern Chile trench sediments and their recycling in arc magmas of the Southern Andes. J. Geol. Soc. 160, 57–70.

Kinny, P.D., Maas, R., 2003. Lu–Hf and Sm–Nd isotope systems in zircon. Rev. Mineral. Geochem. 53 (1), 327–341.

Kotov, A.B., Kozakov, I.K., Bibikova, E.V., Sal'nikova, E.B., Kirnozova, T.I., Kovach, V.P., 1995. Duration of regional metamorphic episodes in areas of polycyclic endogenic processes: a U–Pb geochronological study. Petrology 3, 621–630.

Kovalenko, V.I., Yarmolyuk, V.V., Kovach, V.P., Kotov, A.B., Kozakov, I.K., Salnikova, E.B., Larin, A.M., 2004. Isotope provinces, mechanisms of generation and sources of the continental crust in the Central Asian mobile belt: geological and isotopic evidence. J. Asian Earth Sci. 23, 605–627.

Kovalenko, V.I., Yarmolyuk, V.V., Tomurtogoo, O., Antipin, V.S., Kovach, V.P., Kotov, A.B., Kudryashova, E.B., Sal'nikova, E.B., Zagornaya, N.Y., 2005. Geodynamics and crust-forming processes in the early Caledonides of the Bayanhongor Zone, central Mongolia. Geotectonics 39, 298–316.

Kozakov, I.K., Kotov, A.B., Kovach, V.P., Sal'nikova, E.B., 1997. Crustal growth in the geological evolution of the Baidarik block, central Mongolia: evidence from Sm–Nd isotopic systematics. Petrology 5 (3), 201–207 (Translated from Petrologiya 5 227–235).

Kozakov, I.K., Kotov, A.B., Sal'nikova, E.B., Kovach, V.P., Nutman, A., Bibikova, E.V., Kirnozova, T.I., Todt, W., Kröner, A., Yakovleva, S.Z., Lebedev, V.I., Sugorakova, A.M., 2001. Timing of the structural evolution of metamorphic rocks in the Tuva-Mongolian Massif. Geotectonics 35, 165–184.

Kozakov, I.K., Sal'nikova, E.B., Yakovleva, S.Z., Plotkina, Y.V., Fedoseenko, A.M., 2006. Vendian metamorphism in the accretionary–collisional structure of central Asia. Doklady Earth Sci. 407, 192–197.

Kozakov, I.K., Sal'nikova, E.B., Kovach, V.P., Yarmolyuk, V.V., Anisimova, I.V., Kozlovsky, A.M., Plotnika, Y.V., Myskova, T.A., Fedoseenko, A.M., Yakovleva, S.Z., Sugorakova, A.M., 2008. Vendian stage in formation of the Early Caledonian Superterrane in Central Asia. Stratigr. Geol. Correl. 16 (4), 360–382.

Kröner, A., Windley, B.F., Badarch, G., Tomurtogoo, O., Hegner, E., Jahn, B.M., Gruschka, S., Khain, E.V., Demoux, A., Wingate, M.T.D., 2007. Accretionary growth and crust formation in the Central Asian Orogenic Belt and comparison with the Arabian-Nubian shield. Geol. Soc. Am. Mem. 200, 181–209.

Kröner, A., Demoux, A., Zack, T., Rojas-Agramonte, Y., Jian, P., Tomurhuu, D., Barth, M., 2011. Zircon ages for a felsic volcanic rock and arc-related early Palaeozoic sediments on the margin of the Baydrag microcontinent, Central Asian Orogenic Belt, Mongolia. J. Asian Earth Sci. 42 (5), 1008–1017.

Kurimoto, C., Tungalag, F., Bayarmandal, L., Ichinnorov, N., 1998. K–Ar ages of white micas from pelitic schists of the Bayankhongor area, west Mongolia. Bull. Geol. Surv. Jpn. 49, 19–23.

Langmuir, C.H., Vocke, R.D., Hanson, G.N., Hart, S.R., 1978. A general mixing equation with applications to icelandic basalts. Earth Planet. Sci. Lett. 37, 380–392.

Le Bas, M.J., Le Maitre, R.W., Streckeisen, A., Zanettin, B., 1986. A chemical classification of volcanic rocks based on the total alkali–silica diagram. J. Petrol. 27, 745–750.

Lehmann, J., Schulmann, K., Lexa, O., Corsini, M., Kröner, A., Štípská, P., Tomurhuu, D., Otgonbator, D., 2010. Structural constraints on the evolution of the Central Asian Orogenic Belt in SW Mongolia. Am. J. Sci. 310, 575–628.

Li, X.H., Zhou, H., Chung, S.L., Lo, C.H., Wei, G., Liu, Y., Lee, C.Y., 2002. Geochemical and Sr–Nd isotopic characteristics of late Paleogene ultrapotassic magmatism in southeastern Tibet. Int. Geol. Rev. 44, 559–574.

Li, X.H., Liu, D.Y., Sun, M., Li, W.X., Liang, X.R., Liu, Y., 2004. Precise Sm–Nd and U–Pb isotopic dating of the supergiant Shizhuyuan polymetallic deposit and its host granite, SE China. Geol. Mag. 141, 225–231.

Li, X.H., Li, Z.X., Wingate, M.T.D., Chung, S.L., Liu, Y., Lin, G.C., Li, W.X., 2006. Geochemistry of the 755 Ma Mundine Well dyke swarm, northwestern

Australia: part of a Neoproterozoic mantle superplume beneath Rodinia? Precambr. Res. 146, 1–15.

Li, X.H., Li, W.X., Wang, X.C., Li, Q.L., Liu, Y., Tang, G.Q., 2009. Role of mantle-derived magma in genesis of early Yanshanian granites in the Nanling Range, South China: in situ zircon Hf–O isotopic constraints. Sci. China, Ser. D Earth Sci. 52 (9), 1262–1278.

Li, X.H., Long, W.G., Li, Q.L., Liu, Y., Zheng, Y.F., Yang, Y.H., Chamberlain, K.R., Wan, D.F., Guo, C.H., Wang, X.C., Tao, H., 2010. Penglai zircon megacrysts: a potential new working reference material for microbeam determination of Hf–O isotopes and U–Pb age. Geostand. Geoanal. Res. 34, 117–134.

Li, H., Zhang, H., Ling, M.X., Wang, F.Y., Ding, X., Zhou, J.B., Yang, X.Y., Tu, X.L., Sun, W.D., 2011. Geochemical and zircon U–Pb study of the Huangmeijian A-type granite: implications for geological evolution of the Lower Yangtze River belt. Int. Geol. Rev. 53, 499–525.

Machado, N., Simonetti, A., 2001. U–Pb dating and Hf isotopic composition of zircon by laser ablation–MC–ICP–MS. In: Laser Ablation–ICPMS in the Earth Sciences-Mineralogical Association of Canada Short Course, vol. 29, pp. 121–146.

Maniar, P.D., Piccoli, P.M., 1989. Tectonic discrimination of granitoids. Geol. Soc. Am. Bull. 101, 635–643.

Mitrofanov, F.P., Bibikova, E.V., Gracheva, T.V., Kozakov, I.K., Sumin, L.V., Shuleshko, I.K., 1985. Archaean isotope age of tonalite (grey) gneisses in Caledonian structure of central Mongolia. Doklady Acad. Nauk SSSR 284 (3), 671–674 (in Russian).

Osozawa, S., Tsolmon, G., Majigsuren, U., Sereenen, J., Niitsuma, S., Iwata, N., Pavlis, T., Jahn, B.M., 2008. Structural evolution of the Bayanhongor region, west–central Mongolia. J. Asian Earth Sci. 33 (5), 337–352.

Patiño Douce, A.E., Beard, J.S., 1995. Dehydration–melting of biotite gneiss and quartz amphibolite from 3–15 kbar. J. Petrol. 36, 707–738.

Peccerillo, A., Taylor, S.R., 1976. Geochemistry of Eocene calc-alkaline volcanic rocks from the Kastamonu area, northern Turkey. Contrib. Miner. Petrol. 58 (1), 63–81.

Peng, T.P., Wilde, S.A., Fan, W.M., Peng, B.X., 2013. Late Neoarchean potassic high Ba–Sr granites in the Taishan granite–greenstone terrane: petrogenesis and implications for continental crustal evolution. Chem. Geol. 344, 23–41.

Perugini, D., Poli, G., Christofides, G., Eleftheriadis, G., 2003. Magma mixing in the Sithonia Plutonic Complex, Greece: evidence from mafic microgranular enclaves. Mineral. Petrol. 78, 173–200.

Plank, T., Langmuir, C.H., 1998. The geochemical composition of subducting sediment and its consequences for the crust and mantle. Chem. Geol. 145, 325–344.

Portnyagin, M., Hoernle, K., Plechov, P., Mironov, N., Khubunaya, S., 2007. Constraints on mantle melting and composition and nature of slab components in volcanic arcs from volatiles (H2O, S, Cl, F) and trace elements in melt inclusions from the Kamchatka Arc. Earth Planet. Sci. Lett. 255 (1), 53–69.

Qian, Q., Chung, S.L., Lee, T.Y., Wen, D.J., 2003. Mesozoic high Ba–Sr granitoids from North China: geochemical characteristics and geological implications. Terra Nova 15, 272–278.

Qin, J.F., Lai, S.C., Grapes, R., Diwu, C., Ju, Y.J., Li, Y.F., 2009. Geochemical evidence for origin of magma mixing for the Triassic monzonitic granite and its enclaves at Mishuling in the Qinling orogen (central China). Lithos 112, 259–276.

Rapp, R.P., Watson, E.B., Miller, C.F., 1991. Partial melting of amphibolite/eclogite and the origin of Archean trondhjemites and tonalites. Precambr. Res. 51, 1–25.

Rudnick, R.L., Gao, S., 2003. The composition of the continental crust. In: Rudnick, R.L. (Ed.), The Crust. Elsevier-Pergamon, Oxford, pp. 1–64.

Sengör, A.M.C., Natal'in, B.A., 1996. Turkic-type orogeny and its role in the making of the continental crust. Annu. Rev. Earth Planet. Sci. 24, 263–337.

Sengör, A.M.C., Natal'in, B.A., Burtman, V.S., 1993. Evolution of the Altaid tectonic collage and Paleozoic crustal growth in Eurasia. Nature 364, 299–307.

Soderlund, U., Patchett, P.J., Vervoort, J.D., Isachsen, C.E., 2004. The 176Lu decay constant determined by Lu–Hf and U–Pb isotope systematics of Precambrian mafic intrusions. Earth Planet. Sci. Lett. 219, 311–324.

Sun, S.S., McDonough, W.F., 1989. Chemical and isotopic systematics of oceanic basalts: implications for mantle composition and processes. In: Saunders, A.D., Norry, M.J. (Eds.), Magmatism in the Ocean Basin, vol. 42. Geological Society Special Publication, Blackwell Scientific Publications, pp. 313–346.

Tarney, J., Jones, C.E., 1994. Trace element geochemistry of orogenic igneous rocks and crustal growth models. J. Geol. Soc. London 151, 855–868.

Teraoka, Y., Suzuki, M., Tungalag, F., Ichinnorov, N., Sakamaki, Y., 1996. Tectonic framework of the Bayanhongor area, west Mongolia. Bull. Geol. Soc. Jpn. 47, 447–455.

Thompson, A.B., Connolly, A.D., 1995. Melting of the continental crust: some thermal and petrological constraints on anatexis in continental collision zones and other tectonic settings. J. Geophys. Res. 100, 15565–15579.

Vernon, R.H., 1984. Microgranitoid enclaves in granites: globules of hybrid magma quenched in a plutonic environment. Nature 309, 438–439.

Waight, T.E., Maas, R., Nicholls, I.A., 2000. Fingerprinting feldspar phenocrysts using crystal isotopic composition stratigraphy: implications for crystal transfer and magma mingling in S-type granites. Contrib. Miner. Petrol. 139, 227–239.

Wang, K.L., O'Reilly, S.Y., Kovach, V., Griffin, W.L., Pearson, N.J., Yarmolyuk, V., Kuzmin, M.I., Chieh, C.J., Shellnutt, J.G., Iizuka, Y., 2013. Microcontinents among the accretionary complexes of the Central Asia Orogenic Belt: in situ Re–Os evidence. J. Asian Earth Sci. 62, 37–50.

White, A.J.R., Chappell, B.W., Wyborn, D., 1999. Application of the restite model to the Deddick granodiorite and its enclaves – a reinterpretation of the observations and data of Maas et al. (1997). J. Petrol. 40 (3), 413–421.

Wilson, B.M., 1989. Igneous Petrogenesis. Springer, Harper Collins Academic, London, p. p. 466.

Windley, B.F., Alexeiev, D., Xiao, W.J., Kröner, A., Basarch, G., 2007. Tectonic models for acceretion of the Central Asian Orogenic Belt. J. Geol. Soc. London 164, 31–47.

Xiao, W.J., Windley, B.F., Badarch, G., Sun, S., Li, J., Qin, K.Z., Wang, Z.H., 2004. Palaeozoic accretionary and convergent tectonics of the southern Altaids: implications for the growth of Central Asia. J. Geol. Soc. London 161, 339–342.

Xiao, W.J., Han, C.M., Yuan, C., Sun, M., Lin, S.F., Chen, H.L., Li, Z.L., Li, J.L., Sun, S., 2008. Middle Cambrian to Permian subduction-related accretionary orogenesis of North Xinjiang, NW China: implications for the tectonic evolution of Central Asia. J. Asian Earth Sci. 32, 102–117.

Xiao, W.J., Kröner, A., Windley, B., 2009. Geodynamic evolution of Central Asia in the Paleozoic and Mesozoic. Int. J. Earth Sci. 98, 1185–1188.

Yang, J.H., Wu, F.Y., Wilde, S.A., Xie, L.W., Yang, Y.H., Liu, X.M., 2007. Tracing magma mixing in granite genesis: in situ U–Pb dating and Hf–isotope analysis of zircons. Contrib. Miner. Petrol. 153, 177–190.

Ye, H.M., Li, X.H., Li, Z.X., Zhang, C.L., 2008. Age and origin of high Ba–Sr appinite–granites at the northwestern margin of the Tibet Plateau: implications for early Paleozoic tectonic evolution of the Western Kunlun orogenic belt. Gondwana Res. 13, 126–138.

Yuan, C., Zhou, M.F., Sun, M., Zhao, Y.J., Wilde, S.A., Long, X.P., Yan, D.P., 2010. Triassic granitoids in the eastern Songpan Ganzi Fold Belt, SW China: magmatic response to geodynamics of the deep lithosphere. Earth Planet. Sci. Lett. 290, 481–492.

Zheng, Y.F., Zhang, S.B., Zhao, Z.F., Wu, Y.B., Li, X.H., Li, Z.X., Wu, F.Y., 2007. Contrasting zircon Hf and O isotopes in the two episodes of Neoproterozoic granitoids in South China: implications for growth and reworking of continental crust. Lithos 96, 127–150.